



HAL
open science

Distribution and long-term change of the sea surface carbonate system in the Mozambique Channel (1963-2019)

Claire Lo Monaco, Nicolas Metzl, Jonathan Fin, Claude Mignon, Pascale Cuet, Éric Douville, Marion Gehlen, Thi Tuyet Trang Chau, Aline Tribollet

► **To cite this version:**

Claire Lo Monaco, Nicolas Metzl, Jonathan Fin, Claude Mignon, Pascale Cuet, et al.. Distribution and long-term change of the sea surface carbonate system in the Mozambique Channel (1963-2019). *Deep Sea Research Part II: Topical Studies in Oceanography*, 2021, 186-188, pp.104936. 10.1016/j.dsr2.2021.104936 . hal-03238398

HAL Id: hal-03238398

<https://hal.science/hal-03238398>

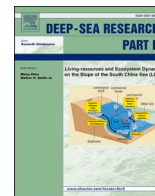
Submitted on 21 Oct 2021

HAL is a multi-disciplinary open access archive for the deposit and dissemination of scientific research documents, whether they are published or not. The documents may come from teaching and research institutions in France or abroad, or from public or private research centers.

L'archive ouverte pluridisciplinaire **HAL**, est destinée au dépôt et à la diffusion de documents scientifiques de niveau recherche, publiés ou non, émanant des établissements d'enseignement et de recherche français ou étrangers, des laboratoires publics ou privés.



Distributed under a Creative Commons Attribution - NonCommercial - NoDerivatives 4.0 International License



Distribution and long-term change of the sea surface carbonate system in the Mozambique Channel (1963–2019)

Claire Lo Monaco^a, Nicolas Metzler^{a,*}, Jonathan Fin^a, Claude Mignon^a, Pascale Cuet^b, Eric Douville^c, Marion Gehlen^c, Thi Tuyet Trang Chau^c, Aline Tribollet^a

^a Laboratoire LOCEAN/IPSL, Sorbonne Université-CNRS-IRD-MNHN, Paris, 75005, France

^b Laboratoire ENTROPIE and Laboratoire d'Excellence CORAIL, Université de La Réunion-IRD- CNRS-IFREMER-Université de la Nouvelle-Calédonie, Saint-Denis, La Réunion, 97744, France

^c Laboratoire LSCE/IPSL, CEA-CNRS-UVSQ, Université Paris-Saclay Gif-sur-Yvette, 91191, France

ARTICLE INFO

Keywords:

Mozambique Channel
Ocean CO₂
Acidification
Long-term trends

ABSTRACT

We report new oceanic carbonate system observations obtained during two cruises conducted in January 2004 (OISO-11) and April 2019 (CLIM-EPARSEs) in the Mozambique Channel and estimate the long-term trend of sea surface fugacity of CO₂ (fCO₂) and pH using historical data. While in January 2004 the region was a large CO₂ source, the ocean was near equilibrium in April 2019. Although this region experienced a dramatic cyclone event “Idai” in March 2019 leading to low salinity and low dissolved inorganic carbon (C_T) and total alkalinity (A_T) concentrations in the central channel, salinity normalized A_T were unchanged and C_T concentrations were higher in 2019 compared to 2004 by about 12 μmol.kg⁻¹, likely due to anthropogenic CO₂ uptake over 15 years. Compared to fCO₂ observations of 1963 in the channel, the oceanic fCO₂ was higher in 2004/2019 by about 100 μatm, an increase close to that observed in the atmosphere (90 ppm). A part of the fCO₂ increase from 1963 to 2019 (about +10 μatm) is due to the long-term ocean warming in this region (+0.011 °C.decade⁻¹). We estimated a mean decrease of -0.087 (±0.007) pH unit between 1963 and 2019, typical of the preindustrial versus modern change in the global ocean. Using other observations in the southern part of the Mozambique Channel (around 25°S) we estimated a pH trend of -0.0129.decade⁻¹ (±0.0042) for 1963–1995 and -0.0227.decade⁻¹ (±0.0048) for 1995–2019 suggesting a strengthening of acidification trend in the Mozambique Channel in agreement with the anthropogenic CO₂ forcing. For the recent period, these rates were confirmed by reconstructed fCO₂ and pH monthly fields using a neural network model. We noted however that the pH trend in the Mozambique Channel appeared lower than previous estimates at the scale of the Indian Ocean. Based on historical atmospheric CO₂ data we estimated that pH in the Mozambique Channel was about 8.18 (±0.014) in the year 1800, i.e. 0.13 higher than in 2019. The concentration of C_T in the year 1800 was likely around 1915 (±10) μmol.kg⁻¹. These results will contribute to a better understanding of the impacts of ocean acidification on coral reefs since the industrial revolution by (1) providing a reference level for the reconstruction of pH from coral core samples that were collected at different locations in this region in 2019 and (2) by informing environmental authorities aiming at preserving and protecting those threatened ecosystems.

1. Introduction

Since the industrial revolution, about 675 GtC of anthropogenic carbon dioxide (CO₂) has been emitted into the atmosphere (Friedlingstein et al., 2019) leading to an unprecedented growth of atmospheric CO₂ concentrations that reached on average 410 ppm in 2019 (Dlugokencky and Tans, 2020). Since 1750 about 25% of anthropogenic CO₂

has been absorbed by the ocean (Friedlingstein et al., 2019) and about 31% during the period 1994–2007 (Gruber et al., 2019a). This absorption helps to mitigate global warming but induces ocean acidification (Doney et al., 2009; Feely et al., 2009; Wu et al., 2018). The latter is a major threat to marine ecosystems (Fabry et al., 2008; Gattuso et al., 2015). It impacts both calcifying organisms such as coccolithophores (Riebesell et al., 2000; Beaufort et al., 2011), foraminifera (de Moel

* Corresponding author. Laboratoire LOCEAN – IPSL - UMR 7159 CNRS/IRD/SU/MNHN, Sorbonne Université, Case 100 - 4 Place Jussieu, 75252, Paris cedex 05, France.

E-mail address: nicolas.metzler@locean.ipsl.fr (N. Metzler).

<https://doi.org/10.1016/j.dsr2.2021.104936>

Received 31 July 2020; Received in revised form 1 April 2021; Accepted 5 May 2021

Available online 25 May 2021

0967-0645/© 2021 The Authors.

Published by Elsevier Ltd.

This is an open access article under the CC BY-NC-ND license

(<http://creativecommons.org/licenses/by-nc-nd/4.0/>).

et al., 2009), bivalves (Waldbusser et al., 2015; Tan and Zheng, 2020), and corals (Kleypas et al., 1999; Mollica et al., 2018), and major agents of carbonate dissolution, the bioeroding microflora and sponges (Schönberg et al., 2017). The accumulation of anthropogenic CO₂ in the ocean has led to a global decrease in pH in surface waters by on average -0.1 units since the industrial revolution (Jiang et al., 2019). It is projected to further decrease by on average -0.2 to -0.4 units by the end of the century depending on the anthropogenic emission scenario and locations (Orr et al., 2005; Jiang et al., 2019; IPCC, 2019). Although future pH changes appear to be more pronounced in the cold and high latitudes (especially in the Arctic) compared to equatorial upwelling areas, significant pH changes are also likely to occur in the tropics and subtropics (Jiang et al., 2019; Ono et al., 2019).

Long-term observations at fixed open ocean monitoring stations since the 1980s or the 1990s show that ocean pH declined between -0.0013 and -0.0026 units per year depending on the location (Bates et al., 2014). High rates of surface ocean acidification are reported for coastal zones, ranging from -0.0020 .yr⁻¹ (± 0.0007) off the south coast of Japan (Ishii et al., 2011) to -0.0028 .yr⁻¹ (± 0.0003) in the Mediterranean Sea (Kapsenberg et al., 2017). In coral reef areas, high-frequency variability (e.g. Hofmann et al., 2011; Cyronak et al., 2020) confounds the assessment of the long-term pH trend by direct measurements. However, pH time series reconstructed based on coral boron isotopic ratio ($\delta^{11}\text{B}$) allow to identify a prominent ocean acidification trend in the recent decades (e.g. Liu et al., 2014; Wu et al., 2018; D’Olivo et al., 2019). A compilation of direct pCO₂ observations at several coral reef locations (Cyronak et al., 2014) suggests that over 1992–2012 sea water pCO₂ increased at a rate of $+6.6$ (± 1.4) $\mu\text{atm.yr}^{-1}$,

i.e. up to times 3.5 faster than in the atmosphere and the open ocean. At constant temperature and alkalinity this would lead to a fast pH decline of -0.0055 .yr⁻¹ in coral reef areas against -0.0018 .yr⁻¹ on average in the open ocean (Feely et al., 2009; Lauvset et al., 2015; Iida et al., 2020) ultimately triggering net dissolution of reef structures (Eyre et al., 2018; Tribollet et al., 2019). At global scale, based on high quality surface ocean fCO₂ data compiled in the SOCAT data product version 2 (Bakker et al., 2014; Pfeil et al., 2013), and combined with regional alkalinity/salinity relationships (Lee et al., 2006), Lauvset et al. (2015) estimated rates of pH declines ranging from -0.0010 .yr⁻¹ to -0.0027 .yr⁻¹ in different basins over the period 1991–2011. The fastest pH decline of -0.0024 .yr⁻¹ (± 0.0004) for the period 1981–2011 and of -0.0027 .yr⁻¹ (± 0.0005) over 1991–2011 occurred in the Indian Ocean. In addition to ocean warming, such a rapid pH change, if confirmed by independent measurements and correlated to a rapid change of the carbonate saturation state, might put Indian Ocean coral reef ecosystems at risk, including many of those in the Mozambique Channel (e.g. Eparses Islands). In this oceanic region, *in situ* observations remain scarce as very few oceanographic campaigns have been conducted.

Here we present the first temporal observations of the sea surface carbonate system in the Mozambique Channel (including fugacity of CO₂, fCO₂, total alkalinity, A_T and dissolved inorganic carbon, C_T) measured during two cruises conducted in January 2004 and April 2019. We also use historical fCO₂ observations to explore the long-term change in fCO₂ and pH in this region over the period 1963–2019 and compare these variations with estimates of regional anthropogenic CO₂ concentrations and with reconstructed monthly pCO₂ and pH fields derived from a neural network model (Denvil-Sommer et al., 2019; Chau

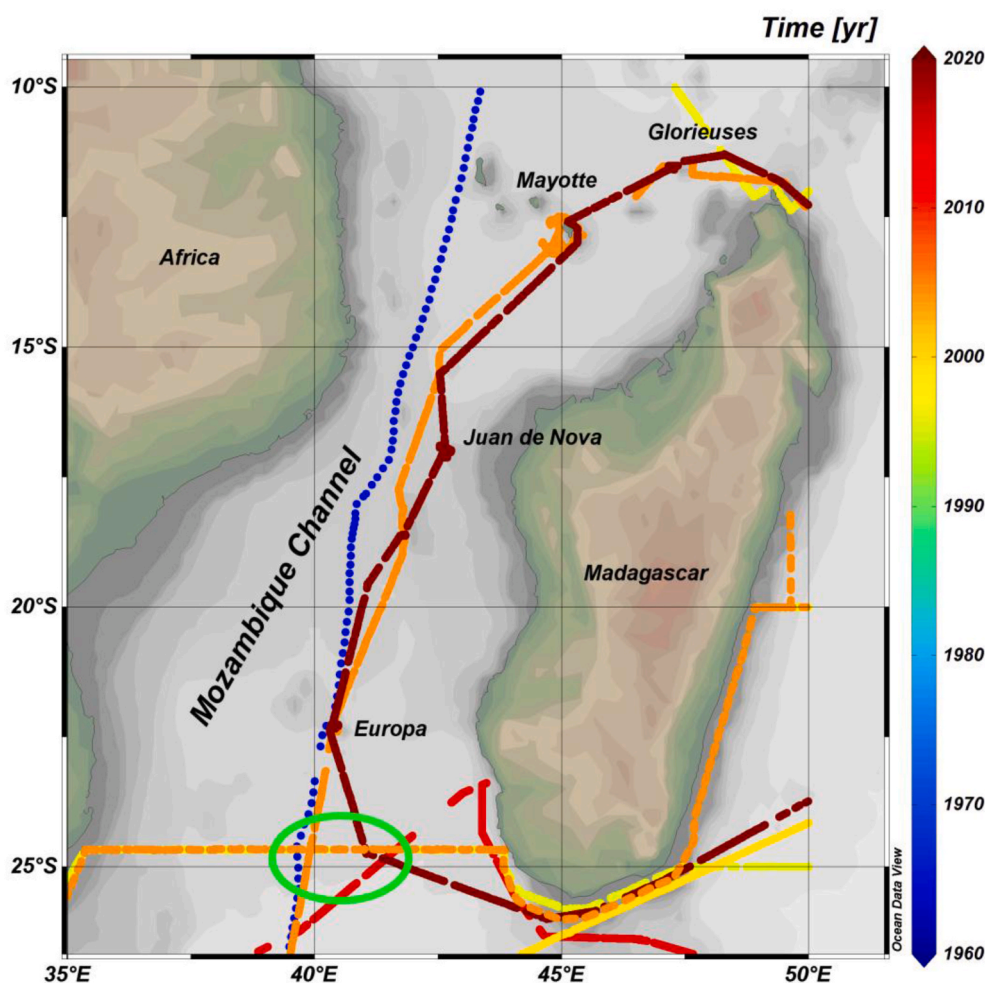


Fig. 1. Cruises in the Mozambique Channel included to the SOCAT data product (version v2020, www.socat.info, Bakker et al., 2016, 2020). Color code is for Year. In the Mozambique Channel, cruises for May 1963 (in blue), January 2004 (OISO-11, in orange), April 2019 (CLIM-EPARSEs, in brown). Water-column data from GLODAP at 25°S were collected in Jun-1995 (yellow) and Dec-2003 (orange). All cruises used in this study are listed in Table 1. Figure produced with ODV (Schlitzer, 2013).

et al., 2020).

2. Data collection and methods

2.1. Observations during the 2004 and 2019 cruises

In January 2004 (Cruise OISO-11, 8-Jan/7-Feb 2004) and April 2019 (project CLIM-EPARSEs, 5–30 April 2019) we conducted two cruises in the Mozambique Channel on-board R.V. Marion-Dufresne (Fig. 1, Table 1). During these cruises, underway continuous surface ocean measurements were made for temperature (SST), salinity (SSS), fugacity of CO₂ (fCO₂), total alkalinity (A_T) and total dissolved inorganic carbon (C_T). In addition, discrete sea surface samples were taken for the analysis of Chl-a and nutrients. In April 2019, the sampling scheme was completed by hydrocasts at selected stations (0–200m in coastal waters nearby the Eparses Islands, and 0–1000m in open waters between islands). With the exception of Chl-a, analytical methods follow the protocol used since 1998 during OISO cruises onboard R.V. Marion-Dufresne in the Southern Indian Ocean. They have been previously described (Jabaud-Jan et al., 2004; Metzl et al., 2006; Metzl, 2009).

Sea surface temperature (SST) and salinity (SSS) were measured continuously using a SBE45 thermosalinograph. Salinity data were controlled by regular sampling and conductivity measurements (Guideline Autosol 8400B and using IAPSO standard/OSIL). Sea surface temperature and salinity were also checked against CTD's surface records. Accuracies of SST and SSS are about 0.005 °C and 0.01.

In addition to the continuous underway measurements, we regularly sampled surface water for Chlorophyll-a (Chl-a) and nutrients (Nitrate and Silicate). The Chl-a samples were stored at –80 °C on-board after filtration and measured back in the laboratory using a fluorometric method (Aminot and K  rouel, 2004). Nitrate and silicate were measured onboard in January 2004 with an automatic colorimetric Technicon analyser following the methods described by Tr  guer and Le Corre (1975).

Total alkalinity (A_T) and total dissolved inorganic carbon (C_T) were measured on-board for both underway continuous surface and water-column samples using a potentiometric titration method (Edmond, 1970) in a closed cell. The system is automatic for sampling continuously surface seawater and transferring it into the cell. For water-column

Table 1

List of cruises in the Mozambique Channel (10°S–25°S) used in this study for surface fCO₂ data (SOCAT, version v2020, Bakker et al., 2016, 2020) and for A_T/C_T water column at 25°S (GLODAPv2.2019, Olsen et al., 2019).

Data-Base	Expocode	Period	Region	PI or Reference
		Month-Year	(Lat. Band)	
Surface Underway fCO₂				
SOCAT-v2020	31AR19630216	May-1963	10°S-27°S	Keeling and Waterman (1968)
SOCAT-v2020	316N19950611	Jun-1995	at 25°S	Key R
SOCAT-v2020	49NZ20031209	Dec-2003	at 25°S	Murata A.
SOCAT-v2020	35MV20040106	Jan-2004	10°S-27°S	Metzl (2009) and this study ^(a)
SOCAT-v2020	06BE20140710	Jul-2014	at 25°S	Steinhoff, T., Koertzing, A
SOCAT-v2020	35MV20190405	Apr-2019	10°S-27°S	This Study ^a
Hydrocast stations (with C_T and A_T in water column)				
GLODAPv2-2019	316N19950611	Jun-1995	at 25°S	Sabine et al. (1999)
GLODAPv2-2019	49NZ20031209	Dec-2003	at 25°S	Murata et al. (2010)

(a) In January 2004 and April 2019 A_T and C_T were also measured underway.

measurements, samples were collected from Niskin bottles in 500 ml glass bottles for analysis within 4h or by adding 300 µl of saturated mercuric chloride solution before storage in a cool place for subsequent analysis. For calibration, we used the Certified Referenced Materials (CRMs, Batch #52, 58 and 62 for OISO-11 and Batch #173 for CLIM-EPARSEs) provided by Pr. A. Dickson (SIO, University of California). For both cruises, we estimated the accuracy at about 3 µmol kg⁻¹ for both A_T and C_T (based on CRMs measurements). During CLIM-EPARSEs standard errors of 122 replicates for surface samples were ±2.6 µmol kg⁻¹ for A_T and ±2.4 µmol kg⁻¹ for C_T. For OISO-11, a cruise that took place in January–February 2004 in the Mozambique Channel and the Southern Indian ocean (including 15 stations), errors of replicates for deep samples (n = 19) was ±2.7 µmol kg⁻¹ for A_T and ±3.3 µmol kg⁻¹ for C_T. Errors of 31 replicates for surface samples were ±1.5 µmol kg⁻¹ for A_T and ±1.8 µmol kg⁻¹ for C_T. The water column data for OISO-11 have been quality controlled in CARINA (Lo Monaco et al., 2010) and revisited in GLODAPv2 (Key et al., 2015; Olsen et al., 2016) with no corrections applied for A_T and C_T. Surface underway A_T and C_T data for OISO-11 and CLIM-EPARSEs are both available at NCEID/OCADS (Metzl and Lo Monaco, 2018; Lo Monaco et al., 2020b).

During CLIM-EPARSEs in April 2019, one station located at 22.30°S/40.40°E was sampled near Europa Island. At 1000m, our measurements for A_T and C_T data are respectively 2334 µmol kg⁻¹ and 2247 µmol kg⁻¹. We are not aware of any biogeochemical stations (including A_T and C_T data) in the central Mozambique Channel. However a WOCE line was sampled in the southern part at 25°S in June 1995 (Sabine et al., 1999) and reoccupied in December 2003 (Murata et al., 2010). These data are part of the GLODAPv2.2019 data product (Olsen et al., 2019). At 25°S around 1000m GLODAPv2.2019 data were in a range of 2310–2340 µmol kg⁻¹ for A_T and 2200–2255 µmol kg⁻¹ for C_T. Our measurements at 1000m at 22.30°S in 2019 are thus in the higher range of concentrations observed at 25°S in 1995 or 2003, not taking into account the natural variability and anthropogenic signals.

For fCO₂ measurements, sea-surface water was continuously equilibrated with a “thin film” type equilibrator thermostated with surface seawater (Poisson et al., 1993). The CO₂ in the dried gas was measured with a non-dispersive infrared analyser (NDIR, Siemens Ultramat 5F or 6F). Standard gases for calibration (around 270, 350 and 480 ppm) and atmospheric CO₂ were measured every 6 h. To correct xCO₂ dry measurements to fCO₂ *in situ* data, we used polynomials given by Weiss and Price (1980) for vapour pressure and by Copin-Mont  gut (1988, 1989) for temperature (temperature in the equilibrium cell was on average 0.73 °C warmer than SST during OISO-11 and 0.097 °C warmer during CLIM-EPARSEs). The oceanic fCO₂ for both cruises are available in SOCAT data product (version v2020, Bakker et al., 2016, 2020) and at NCEID/OCADS (Metzl, 2018; Lo Monaco et al., 2020a). Note that when added to SOCAT, original fCO₂ data are recomputed (Pfeil et al., 2013) using temperature correction from Takahashi et al. (1993). Given the small difference between SST and equilibrium temperature, the fCO₂ data from our cruises are identical (within 1 µatm) in SOCAT and NCEID/OCADS. For coherence with other cruises we therefore used fCO₂ values as provided by SOCAT.

Atmospheric xCO₂ measured on-board was on average 377.02 (±0.73) ppm in January 2004 and 410.90 (±1.40) ppm in April 2019 in the Mozambique Channel (Supp. Fig. 1). This corresponds to an increase of +33.9 ppm in 15 years, coherent with global atmospheric xCO₂ values. Our measurements on board in this specific region (10°S–26°S) are almost identical to the global averaged marine surface monthly mean xCO₂ of 377.04 ppm for January 2004 and 411.06 ppm for April 2019 (Dlugokencky and Tans, 2020). The relatively large standard-deviation of atmospheric xCO₂ encountered in the Mozambique Channel (up to ± 1.4 ppm in 2019) compared to other OISO cruises in the Southern Indian Ocean (Metzl, 2009) is likely linked to the terrestrial signal from Africa and/or Madagascar depending on the season and wind fields. However given the increase of atmospheric xCO₂ over 15 years, the observed regional atmospheric xCO₂ variability

during each cruise had no significant impact on the air-sea CO₂ disequilibrium that we explored in this study. We thus used the mean xCO₂ values for each cruise (377 and 411 ppm) and converted xCO₂ to fCO₂ at 100% humidity following Weiss and Price (1980) for air-sea disequilibrium estimates.

2.2. Other observations and data

In order to investigate the long-term variability of fCO₂ and pH we used all fCO₂ data available in the Mozambique Channel from the SOCAT data product (version v2020, Bakker et al., 2016, 2020): our observations for 2004 and 2019 and the only other cruise conducted in the Channel in May 1963 (Keeling and Waterman, 1968). These three cruises offer a first view of fCO₂ variations over several decades in the Mozambique Channel, between 14°S and 25°S. However, because they are representative of different seasons (January, April and May) we included fCO₂ data collected in the southern part of the Channel at around 25°S to confirm the fCO₂ and pH trends over decades deduced in the band 14°S–25°S. All the cruises used in this study are shown in Fig. 1 (listed in Table 1) from which we select only recommended fCO₂ data (with WOCE Flag 2 in SOCAT). In addition, in order to separate the natural and anthropogenic CO₂ signals, we used water-column data from June 1995 and December 2003 along 25°S (Sabine et al., 1999; Murata et al., 2010) quality controlled in GLODAPv2.2019 (Olsen et al., 2019). Our estimates of anthropogenic CO₂ (hereafter C_{ant}) in this region will be compared to a recent evaluation of C_{ant} inventory changes in the global ocean between 1994 and 2007 (Gruber et al., 2019a;b). To discuss the seasonality of the carbonate system and air-sea CO₂ fluxes in this region we will also compare our observations with the climatology produced by Takahashi et al. (2009, 2014). Finally, we will compare our results with reconstructed pCO₂ and pH monthly fields for the period 1985–2019 derived from a neural network model (named CMEMS-LSCE-FFNN, Denvil-Sommer et al., 2019; Chau et al., 2020).

2.3. Calculations of carbonate system properties and anthropogenic carbon

Based on the carbonate properties available for each cruise (fCO₂, A_T and C_T) other carbonate system properties (like pH, [H⁺] or the carbonate saturation state Ω) are calculated using the CO2sys program (version CO2sys_v2.5, Orr et al., 2018) developed by Lewis and Wallace (1998) and adapted by Pierrot et al. (2006) with K1 and K2 dissociation constants from Lueker et al. (2000) and KSO₄ constant from Dickson (1990). The total boron concentration is calculated according to Uppström (1974). We have tested different K1, K2 constants (Merbach et al., 1973; Hansson, 1973; Dickson and Millero, 1987) and compared measured fCO₂ with fCO₂ calculated from A_T/C_T pairs collocated in space and time (Supp. Figs. S2a and b). Given the uncertainties associated to the measurements of temperature (0.005 °C), salinity (0.01), A_T and C_T (2.5 μmol kg⁻¹), the error on calculated fCO₂ is ±13 μatm. This error is generally larger than the mean differences observed between measured and calculated fCO₂ (Supp. Fig. S2b). For example, the average differences between measured and calculated fCO₂ when using K1, K2 constants from Lueker et al. (2000) were -5.3 (std ±4.9) μatm for 154 co-located samples in January 2004, and +4.5 (std ±5.2) μatm for 268 co-located samples in April 2019. In line with previous recommendations (Dickson et al., 2007; Orr et al., 2015) we used constants from Lueker et al. (2000) for all calculations. To account for the effect of salinity on A_T and C_T concentrations these properties are also normalized at constant salinity (35) following N-A_T = A_T * 35/SSS and N-C_T = C_T * 35/SSS. In this study we are interested in evaluating fCO₂ variations over several decades. As fCO₂ is highly dependent on SST, fCO₂ will be also normalized at constant temperature (29 °C) following the relation established by Takahashi et al. (1993).

$$fCO_{29} = fCO_{2SST} * EXP(0.0423*(29-SST)) \quad (1)$$

For anthropogenic CO₂ calculations in the water column (C_{ant}) we used the TrOCA method (Touratier et al., 2007) that was previously applied and compared to other methods in the Southern Indian Ocean along the 32°S section (Álvarez et al., 2009). In short, given A_T, C_T, Oxygen (O₂) and potential temperature (θ) observations at each depth level, the C_{ant} concentrations is derived from the evolution of the quasi-conservative tracer TrOCA compared to its pre-industrial value (see Touratier et al., 2007 for a full description). The final expression used to calculate C_{ant} is:

$$C_{ant} = \frac{O_2 + 1,279 \left(C_T - \frac{1}{2} A_T \right) - e^{\left[\frac{7,511 - (1,087 \cdot 10^{-2}) \cdot \theta - \frac{7,81 \cdot 10^5}{A_T^2} \right]}{1,279}} \quad (2)$$

To compare with the observed C_T long-term trend in surface waters and given the uncertainty on C_{ant} of ±6.25 μmol kg⁻¹ using the TrOCA method (Touratier et al., 2007) our interpretations in the Mozambique Channel region will be limited to the upper layers (150–200m). In the Southern Indian subtropical region C_{ant} concentrations are generally less than 10 μmol kg⁻¹ below 1000m (Sabine et al., 1999; Álvarez et al., 2009) and C_{ant} accumulation between 1994 and 2007 less than 10 μmol kg⁻¹ below 500 m (Murata et al., 2010; Gruber et al., 2019a).

2.4. Neural network reconstruction of the surface ocean carbonate system

Surface ocean partial pressure of carbon dioxide (pCO₂) is obtained from an ensemble-based feed-forward neural network (FFNN) model described in Denvil-Sommer et al. (2019). For this study, we used results of the latest version of the model (Chau et al., 2020) which was developed as part of the Copernicus Marine Environment Monitoring Service (CMEMS). The mean pCO₂ of a 100 member ensemble is used for comparison and trend analysis throughout this study. Surface ocean pH is computed from reconstructed pCO₂ and alkalinity with the speciation software CO2sys-MATLAB_V2.05 (Van Heuven et al., 2011; Orr et al., 2018). The multivariate linear regression model LIAR (Carter et al., 2016; 2018) is used to derive time and space varying surface ocean alkalinity fields as a function of sea surface temperature and salinity, as well as climatological monthly mean nitrate and dissolved silica concentrations from the World Ocean Atlas 2013 version 2 (Garcia et al., 2014; www.nodc.noaa.gov/OC5/woa13/). Global surface ocean pCO₂ and pH reconstructions at 1° × 1° resolution start in 1985 and are updated annually in phase with yearly releases of SOCAT data. Here we used the SOCAT version v2020 (Bakker et al., 2020) and the model fields calculated for the period 1985–2019. For a full description, access to the data and a statistical evaluation of pCO₂ and pH reconstructions please refer to Chau et al. (2020).

3. Results

3.1. Surface properties observed in January 2004 and April 2019 in the Mozambique Channel

3.1.1. Distributions along the Mozambique Channel

Here we first present the description of sea surface observations obtained in January 2004 and April 2019 in the Mozambique Channel. Underway measurements of SST, SSS and fCO₂ are shown in Fig. 2 while A_T and C_T observations are presented in Fig. 3. Averaged values in the band 14–25°S are listed in Table 2.

During both cruises SST presents a gradual increase from south to north (Fig. 2a). SST was generally higher in January 2004 than in April 2019 except in the South (26°S) and in the North (14°S) of the Channel. In January 2004, SST reached the maximum value of 30 °C at 22°S and was quite homogeneous in the band 14°S–22°S, whereas in April 2019, SST increased more gradually to reach 30.5 °C north of Madagascar. We observed large SST and SSS variability in the central part of the Channel

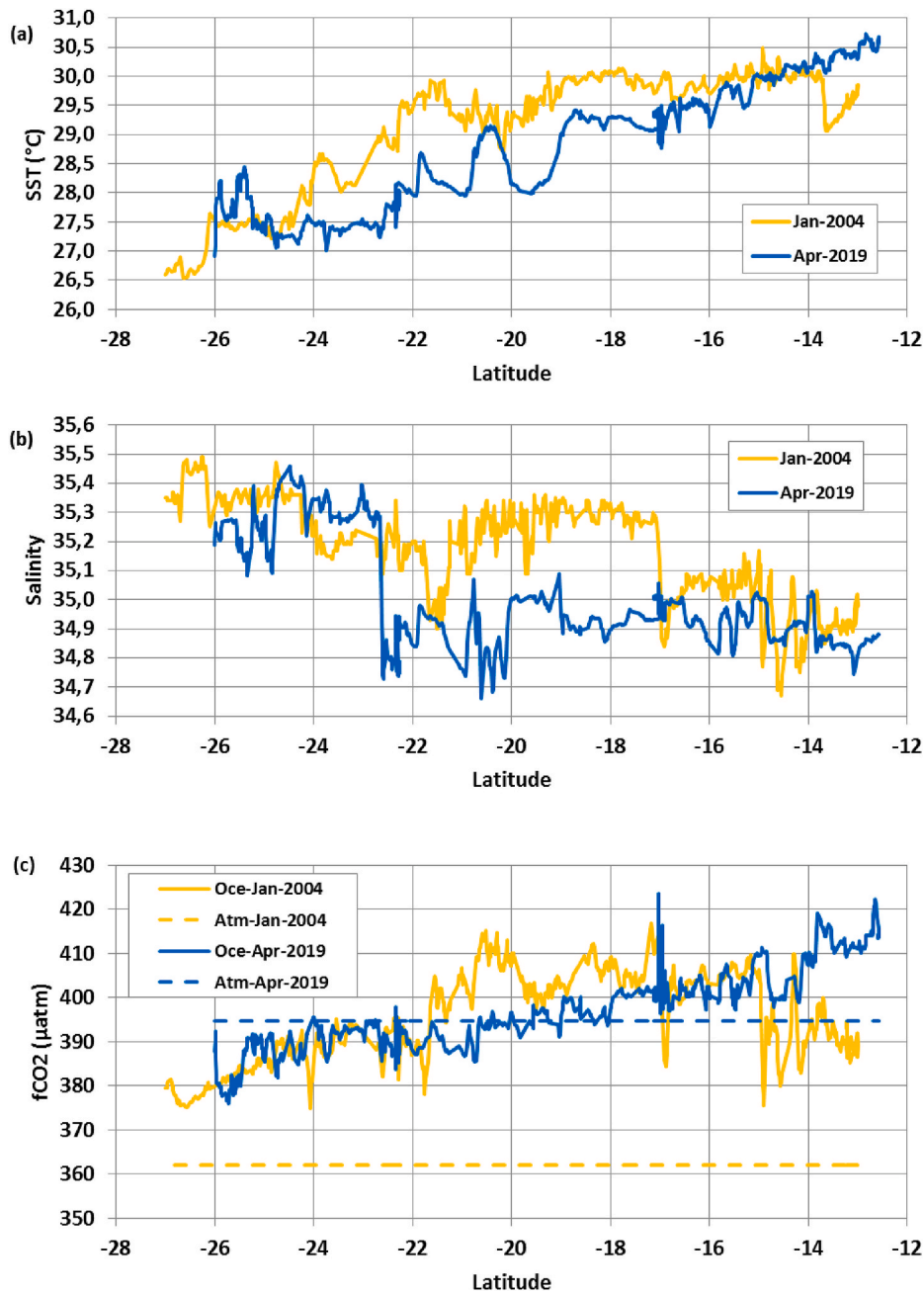


Fig. 2. Sea surface temperature (a), salinity (b) and fCO₂ (c) in the Mozambique Channel observed in January 2004 (orange) and April 2019 (blue). In (c) the dashed lines correspond to atmospheric fCO₂. All underway data, including near Islands are shown.

(18°S–22°S) probably linked to eddies occurring regularly in this region (Halo et al., 2014; Hancke et al., 2014; TERNON et al., 2014). This was well identified from one drifting buoy migrating southwards with an anticyclonic eddy in March–April 2019 (Supp. Fig. S3). The SST and SSS variability in the central part of the Channel is also recognized in A_T and C_T distributions (Fig. 3) but not in fCO₂ (Fig. 2c) because the effects of A_T and C_T on fCO₂ offset each other.

During each cruise, we observed a sharp front of salinity in the central part of the Mozambique Channel that was not associated to a change in SST: in January 2004 the front was located around 17°S (near Juan de Nova Island) whereas it was found at 22.5°S in April 2019 (south of Europa Island). Although the salinity was about the same in 2004 and 2019 in the South and the North of the channel, it was very different in the central region (17°S–23°S, Fig. 2b). The low salinity (SSS < 35) observed in April 2019 was linked to an excess of precipitations

that occurred in March during the dramatic tropical cyclone event called “Idai” (monthly anomaly of precipitation up to 150 mm in the band 18°S–22°S, Supp. Fig. S4). This signal was confirmed by an Argo float (Platform Code 2902142) that recorded salinity as low as 34 in the surface layer in this region in late March 2019 (Supp. Fig. S5).

Precipitations caused by the cyclone Idai directly impacted the concentrations of A_T and C_T which were thus much lower in April 2019 in the central part of the channel (Fig. 3a and b), although one would expect an increase in C_T over 15 years due to the accumulation of anthropogenic CO₂. The salinity fronts at 17°S or 22.5°S (depending on the cruise) were also well identified in A_T and C_T (Fig. 3). The salinity normalized A_T ($N-A_T$) and C_T ($N-C_T$) distributions present much less spatial variability than A_T and C_T and are remarkably homogeneous in the Mozambique Channel south of 14°S during each cruise (Fig. 4).

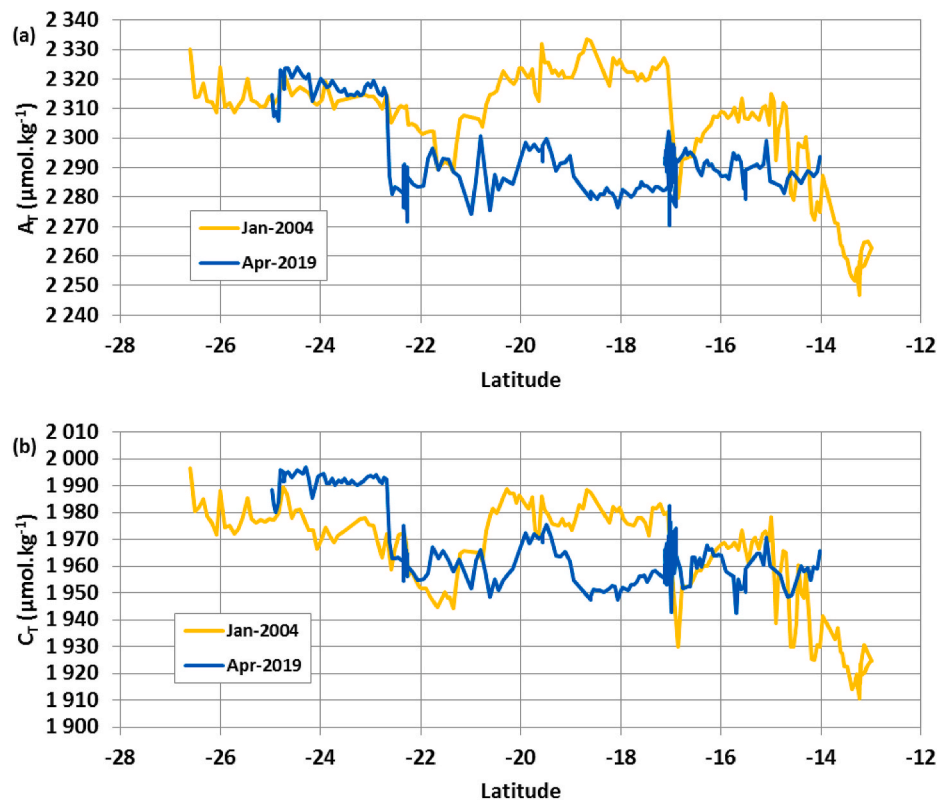


Fig. 3. (a) Sea surface A_T ($\mu\text{mol.kg}^{-1}$) and (b) sea surface C_T ($\mu\text{mol.kg}^{-1}$) in the Mozambique Channel observed in January 2004 (orange) and April 2019 (blue). All underway data, including near Islands are shown.

Table 2

Mean measured, calculated and trends of surface properties in the band 14°S – 25°S based on observations in May 1963, January 2004 and April 2019 in the Mozambique Channel. Nb is the number of data (ND=No Data). Standard deviations are indicated in bracket. Average $N-C_T$ and $N-A_T$ measured only in 2004 and 2019 are also listed to compare with $N-C_T$ and $N-A_T$ calculated with $f\text{CO}_2$ and A_T /SSS relationship. Adjusted values for April 2004 and April 1963 as specified were used to estimate the trends of $f\text{CO}_2$ and $N-C_T$ for different periods. Errors for the trends (in bracket) are based on $f\text{CO}_2$, A_T and C_T measurements uncertainty for each cruise as documented in the main text and Table S1 in Supplementary Material. Last line is the $f\text{CO}_2$ trend without the long-term warming of $+0.011^\circ\text{C.yr}^{-1}$.

Period	Nb	SST °C	$f\text{CO}_2$ μatm	$N-C_{T\text{cal}}$ $\mu\text{mol/kg}$	$N-A_{T\text{cal}}$ $\mu\text{mol/kg}$	Nb	$N-C_{T\text{mes}}$ $\mu\text{mol/kg}$	$N-A_{T\text{mes}}$ $\mu\text{mol/kg}$
April-2019	1677	28.61 (0.83)	397.2 (7.9)	1964.9 (4.4)	2293.1 (1.3)	376	1967.5 (6.9)	2292.8 (4.8)
January-2004	480	29.45 (0.73)	398.9 (8.9)	1958.0 (5.8)	2294.7 (1.3)	142	1955.8 (8.6)	2296.3 (5.8)
May-1963	59	25.77 (1.45)	296.2 (4.9)	1925.7 (10.0)	2292.4 (1.0)	ND	ND	ND
April-2004 (adjusted)			370.8	1949.9			1952.2	
April-1963 (adjusted)			308.1	1908.4			ND	
Trend			$f\text{CO}_2$ $\mu\text{atm.yr}^{-1}$	$N-C_{T\text{cal}}$ $\mu\text{mol.kg}^{-1}.\text{yr}^{-1}$			$N-C_{T\text{mes}}$ $\mu\text{mol.kg}^{-1}.\text{yr}^{-1}$	
2004–2019			+1.75 (0.81)	+1.00 (0.81)			+1.04 (0.79)	
1963–2004			+1.53 (0.28)	+1.00 (0.39)			ND	
1963–2019			+1.58 (0.18)	+1.00 (0.29)			ND	
1963–2019 (without warming)			+1.44 (0.18)					

3.1.2. Differences in A_T and C_T between 2004 and 2019

The largest difference in $N-C_T$ between 2004 and 2019 is observed in the southern part of the channel (21°S – 25°S) where $N-C_T$ concentrations were 10 – $20 \mu\text{mol kg}^{-1}$ higher in April 2019 compared to January 2004 whereas $N-A_T$ values were almost identical for both periods (Fig. 4, Table 2). Given that C_T (and $N-C_T$) climatological annual cycles present higher concentrations in January than in April in the subtropical southern Indian Ocean including the Mozambique Channel (Bates et al., 2006; Takahashi et al., 2014, Supp Fig. S6), the $N-C_T$ average increase of $+11.8 \mu\text{mol kg}^{-1}$ observed between 2004 and 2019 (mean trend of $0.8 \mu\text{mol kg}^{-1}.\text{yr}^{-1}$) likely underestimates the anthropogenic signal. Taking into account the seasonality (based on the C_T climatology computed by Takahashi et al., 2014, Supp Fig. S6), C_T would be $16.9 \mu\text{mol kg}^{-1}$ lower

in April 2004 than in January 2004 ($N-C_T$ in April 2004 would be $1952.2 \mu\text{mol kg}^{-1}$ on average) and the annual increase from April 2004 to April 2019 would be $+1.04 (\pm 0.79) \mu\text{mol.kg}^{-1}.\text{yr}^{-1}$ (Table 2). This number is in the range of the theoretical C_T trend of $+1.2 \mu\text{mol kg}^{-1}.\text{yr}^{-1}$ calculated by assuming that surface ocean $f\text{CO}_2$ follows the atmospheric growth rate observed over 2004–2019 ($+2.2 \text{ppm.yr}^{-1}$). This suggests that most of the increase in $N-C_T$ is due to the accumulation of anthropogenic CO_2 , which could also explain part of the changes in $f\text{CO}_2$ and pH observed between 2004 and 2019, as well as the long-term trends investigated back to the sixties in section 3.2.

3.1.3. $f\text{CO}_2$ variability, seasonality and biological processes

Although the C_T and A_T distributions along the Mozambique Channel

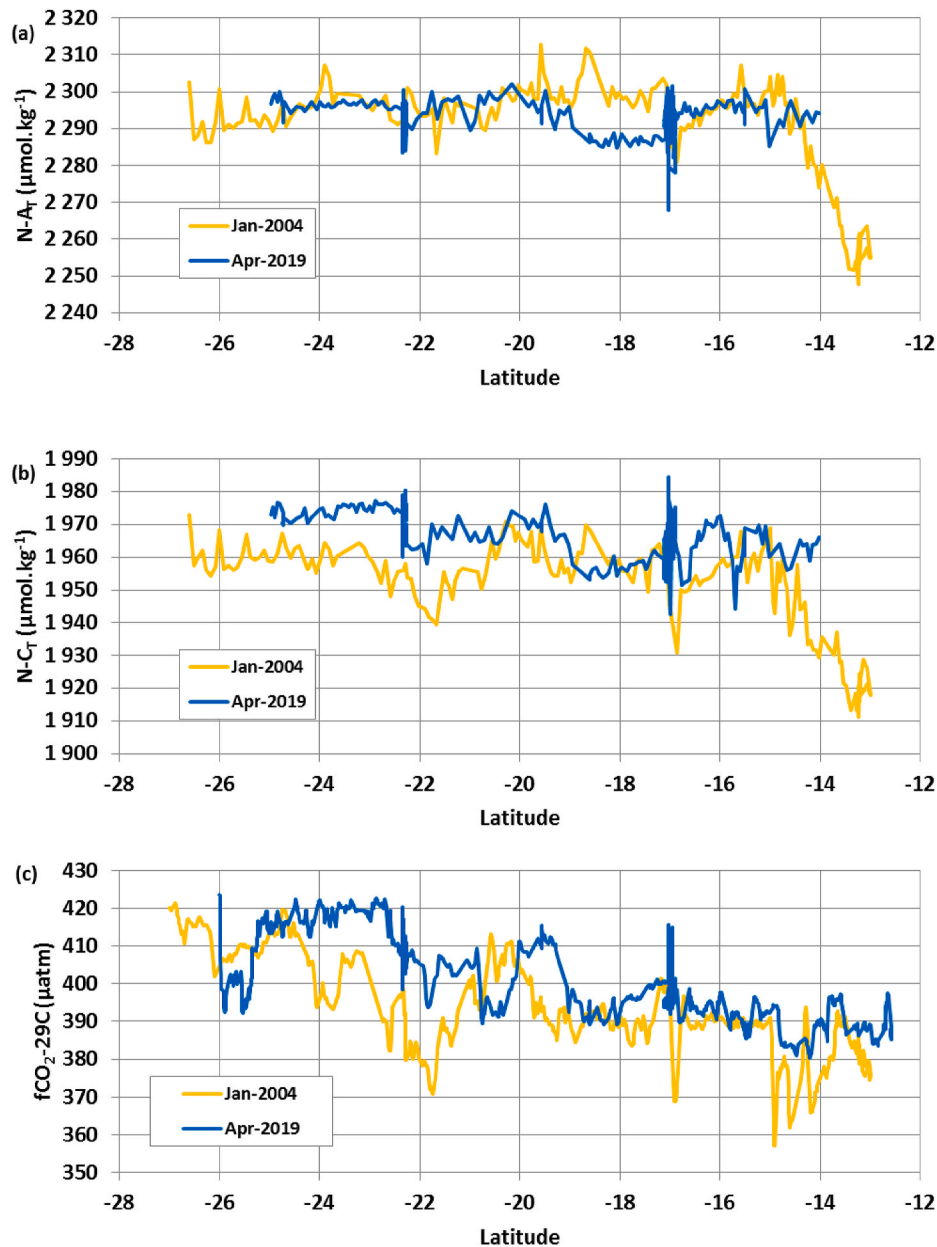


Fig. 4. Same as Fig. 3 for (a) Salinity normalized A_T ($N-A_T$, $\mu\text{mol.kg}^{-1}$) and (b) Salinity normalized C_T ($N-C_T$, $\mu\text{mol.kg}^{-1}$) in the Mozambique Channel observed in January 2004 (orange) and April 2019 (blue). Also presented in (c) the $f\text{CO}_2$ normalized at SST 29 °C ($f\text{CO}_2-29\text{C}$, μatm). All underway data, including near Islands are shown.

present large gradients associated with the salinity fronts at 22.5°S or 17°S (Fig. 3), their impact on $f\text{CO}_2$ cancel each other and the fronts are not recognized in $f\text{CO}_2$ measurements (Fig. 2c). In April 2019, $f\text{CO}_2$ increased progressively northward like SST, leading to a positive $f\text{CO}_2$ /SST relationship, except for measurements conducted in the vicinity of Juan de Nova near 17°S (Supp. Fig. S7). In January 2004, the $f\text{CO}_2$ distribution presented a larger spatial variation leading to a poor relation between $f\text{CO}_2$ and SST (Supp. Fig. S7), notably due to the low $f\text{CO}_2$ values (below 390 μatm) and high SST observed north of 15°S and around 22°S where we also measured minima in C_T (Fig. 3b) and in $N-C_T$ (Fig. 4b). These signals were linked to locally enhanced biological activity revealed in both surface Chl-a *in-situ* measurements around 15°S and 22°S in January 2004 (Supp. Fig. S8) and at regional scale in the monthly Chl-a distribution derived from MODIS (Supp. Fig. S8). In April 2019, *in-situ* Chl-a concentrations were in the same range as in January 2004 with few local maxima also detected around 15°S and 22°S (Supp.

Fig. S8) and also associated with minima in C_T and $N-C_T$ (Figs. 3b and 4b). In the vicinity of the islands (Europa at 22°S and Juan de Nova at 17°S) the Chl-a concentrations in April 2019 present some variability but in the range of observations in the open ocean (0–0.25 mg m^{-3}). High *in-situ* Chl-a concentrations are thus only identified at small-scale during both cruises and these local events do not impact the overall trend of the $f\text{CO}_2$ and C_T changes in the Channel between 2004 and 2019. Instead, satellite derived Chl-a products suggest a rather homogeneous Chl-a distribution and slightly higher values in April 2019 compared to January 2004, notably in the central region (Supp. Fig. S8a). This is reflected in the mean seasonal cycle of Chl-a in this region, suggesting a slight gradual increase of Chl-a from December to July (Supp. Fig. S9). Over the region 15°S–26°S, the average Chl-a concentration derived from MODIS was 0.11 mg m^{-3} in January 2004 and 0.17 mg m^{-3} in April 2019, a mean difference of only 0.06 mg m^{-3} not captured in our *in-situ* localized data (Supp. Fig. S8). In April 2019, the

MODIS Chl-a concentrations of 0.17 mg m^{-3} were the same as the mean climatological value for April ($0.17 \text{ mg m}^{-3} \pm 0.02$ on average for years 2003–2019, Supp. Fig. S9). Thus, although one would expect the cyclone “Idai” that occurred in March 2019 to have impacted primary production (e.g. through input of nutrients either from the subsurface or from terrigenous material through atmospheric transport), we conclude that, except for salinity, observations in April 2019 were close to climatological conditions.

As noted above, climatological C_T concentrations in the channel are on average lower in April than in January (Takahashi et al., 2014) and the $f\text{CO}_2$ decrease from January to April cannot be explained by temperature alone. The seasonal C_T change between winter and summer (up to $30 \mu\text{mol kg}^{-1}$) is likely driven by biological activity but not directly recognized by Chl-a observations (Supp. Fig. S9). This seasonal draw-down of C_T is potentially associated to biological N_2 -fixation similarly to observations in the south-western tropical Pacific where a similar C_T seasonality has been reported (Moutin et al., 2018). In the Western Indian Ocean and the Mozambique Channel *Trichodesmium* blooms (N_2 -fixers) have been detected from satellite data (Westberry and Siegel, 2006). However, the occurrence of blooms from remote sensing data only remains qualitative and obviously limited to large surface aggregations of cells (McKinna, 2015). The hypothesis that diazotrophy may play a significant role in C_T and $f\text{CO}_2$ seasonality is further supported by the observation of high abundances of *Trichodesmium* spp in the Mozambique Channel in April 2011 (Dupuy et al., 2016) but we have no *in-situ* data to document this process during the 2004 and 2019 cruises.

3.1.4. Difference in $f\text{CO}_2$ between 2004 and 2019

Although atmospheric $f\text{CO}_2$ was much higher in 2019 than in 2004, the oceanic $f\text{CO}_2$ range was similar (between 380 and 420 μatm for both periods, Fig. 2c) as well as the mean $f\text{CO}_2$ in the band 14°S – 25°S (Table 2). In January 2004, the ocean $f\text{CO}_2$ was much higher than in the atmosphere (a CO_2 source) with $\Delta f\text{CO}_2$ ($\Delta f\text{CO}_2 = f\text{CO}_{2\text{oc}} - f\text{CO}_{2\text{atm}}$) ranging from 20 to 50 μatm , with a mean value of $+36.8 (\pm 8.9) \mu\text{atm}$. In April 2019, the mean $\Delta f\text{CO}_2$ value was much lower ($+2.5 \pm 7.9$) μatm : the ocean was a CO_2 source north of 18°S (maximum $\Delta f\text{CO}_2$ of $+20 \mu\text{atm}$), near-equilibrium with the atmosphere in the central channel (22°S – 18°S) and a CO_2 sink south of 25°S (minimum $\Delta f\text{CO}_2$ of $-20 \mu\text{atm}$). Not taking into account the increase in oceanic $f\text{CO}_2$ from 2004 to 2019 due to anthropogenic CO_2 uptake, our mean results showing a CO_2 source in January and near-equilibrium in April, are coherent with monthly climatological $\Delta f\text{CO}_2$ values in this region, i.e. $+19.95 (\pm 3.3) \mu\text{atm}$ for January and $+1.2 (\pm 5.3) \mu\text{atm}$ for April (Takahashi et al., 2009). Since very few observations in the Mozambique Channel were used to construct the $p\text{CO}_2$ climatology (Takahashi et al., 2009) our results validate the $p\text{CO}_2$ extrapolation in this region that has been later used to create C_T and pH climatologies (Takahashi et al., 2014).

In the ocean the seasonal variation of $f\text{CO}_2$ is controlled by a complex interplay of thermodynamic, biological, chemical and mixing processes (Takahashi et al., 2002). In the subtropics, including the South Indian Ocean sector, the effect of temperature is generally found to be the dominant process at seasonal (Louanchi et al., 1996; Metzl et al., 1995; Takahashi et al., 2002) and inter-annual scales (Metzl et al., 1998). In order to take into account the thermal effect, observed $f\text{CO}_2$ in January 2004 and April 2019 were normalized to a constant temperature of 29°C ($f\text{CO}_2\text{-}29\text{C}$) close to the average SST observed in January and April. The $f\text{CO}_2\text{-}29\text{C}$ distributions are shown in Fig. 4c. For both periods, $f\text{CO}_2\text{-}29\text{C}$ variations tend to follow the N-C_T distributions (Fig. 4b). As opposed to $f\text{CO}_2$, but like for N-C_T , $f\text{CO}_2\text{-}29\text{C}$ was on average slightly higher in April 2019 ($403.4 \pm 8.5 \mu\text{atm}$) than in January 2004 ($391.9 \pm 10.9 \mu\text{atm}$). The difference of only $+11.5 \mu\text{atm}$ is much lower than the atmospheric increase of $+33.9 \text{ ppm}$ between 2004 and 2019. The temperature drives only part of the $f\text{CO}_2$ monthly variations and it is thus important to correct for other seasonal contributions to evaluate long-term trends in $f\text{CO}_2$. If we adjust the $f\text{CO}_2$ observed in January 2004 to April 2004 based on the climatology (Takahashi et al., 2014, Supp Fig. S6b), $f\text{CO}_2$

data for January are reduced by $28.1 \mu\text{atm}$ and we obtain a mean value of $370.8 \mu\text{atm}$ for April 2004 (Table 2). The $f\text{CO}_2$ increase from April 2004 to April 2019 would lead to a rate of $1.75 (\pm 0.81) \mu\text{atm.yr}^{-1}$ over the last 15 years, slower than $+2.2 \text{ ppm.yr}^{-1}$ in the atmosphere over the same period. At constant A_T the observed increase in $f\text{CO}_2$ would translate into a trend of $+1.01 (\pm 0.45) \mu\text{mol.kg}^{-1}.\text{yr}^{-1}$ in C_T , the same rate deduced from C_T measurements described above ($+1.04 \pm 0.79 \mu\text{mol kg}^{-1}.\text{yr}^{-1}$ for C_T also adjusted to April, Table 2). This simple calculation based on 2 cruises conducted 15 years apart indicates that on average CO_2 concentrations increased in the Mozambique Channel at a rate of around $1.0 \mu\text{mol kg}^{-1}.\text{yr}^{-1}$ and that seasonal signals of $f\text{CO}_2$ and C_T have to be taken into account to properly evaluate the $f\text{CO}_2$ and C_T trends. The same is true when one uses $f\text{CO}_2$ data and A_T /SSS relationship to calculate pH and to evaluate the long-term signal of ocean acidification (e.g. Lauvset et al., 2015).

3.1.5. Selecting the regional A_T /SSS relationship

Similar to what is commonly observed in the global ocean (Millero et al., 1998) there is a strong relationship between A_T and salinity for both cruises (Fig. 5), except in the vicinity of Mayotte Island in January 2004 (north of 14°S). The A_T /SSS relationships are almost the same for January 2004 and April 2019 and close to A_T /SSS relationships derived at large scale in the subtropics or in the Indian Ocean (Millero et al., 1998; Lee et al., 2006). This suggests that these empirical A_T /SSS relationships could be used to reconstruct spatial and temporal distribution of A_T from salinity. In turn, pH can be calculated from reconstructed A_T and $f\text{CO}_2$ data (when only $f\text{CO}_2$ data are available as it is the case for SOCAT, Bakker et al., 2016). In order to select the best A_T /SSS relationship for the Mozambique Channel, we first compared several relations with A_T measurements obtained in January 2004 and April 2019 (Supp. Fig. S10). All relationships, including that of Millero et al. (1998) or Lee et al. (2006), lead to the same residuals with no statistical differences. Therefore, in the following we used the A_T /SSS relationship derived from our observations in 2004 and 2019 (black line in Fig. 5): $A_T (\mu\text{mol.kg}^{-1}) = 73.841 (\pm 1.15) * \text{SSS} - 291.02 (\pm 40.4)$ ($n = 548$, $r^2 = 0.88$).

3.1.6. Detecting recent pH changes in the Mozambique channel

The A_T /SSS relationship described above enables to calculate pH from $f\text{CO}_2$ and SSS underway measurements. Here we are first interested in detecting the change in pH between 2004 and 2019. As we had A_T , C_T and $f\text{CO}_2$ observations for both cruises, we compared pH calculated with A_T and C_T pairs or with $f\text{CO}_2$ and A_T based on the A_T /SSS relationship. Average calculated pH values in the band 14°S – 25°S are listed in Table 3. Both results are presented in Fig. 6 for pH at 29°C (pH-29C). Although calculated pH is subject to uncertainties due to the error in each property (SST, SSS, A_T , C_T or $f\text{CO}_2$) the overall pH-29C distributions are the same either based on A_T - C_T pairs or on underway $f\text{CO}_2$ data. Except in the vicinity of the islands pH-29C values ranged between 8.02 and 8.06. Although pH values at *in-situ* temperature were almost the same (Table 3), pH-29C values were clearly lower in April 2019 compared to January 2004 (Fig. 6, Table 3). On average pH-29C in April 2019 was lower by -0.0116 or -0.0218 depending on the calculation. The pH difference between the 2 cruises reflects both the seasonality and probably the pH decrease due to the accumulation of anthropogenic CO_2 over 15 years. To take into account the seasonality, we adjusted the mean $f\text{CO}_2$ and C_T observation in January 2004 to April 2004 based on the climatology (Takahashi et al., 2014) and recalculate pH adjusted to April 2004 (Table 3). The pH difference between 2019 and 2004 was $-0.0238 (\pm 0.0018)$ (using average $f\text{CO}_2$ data and associated errors) or $-0.0244 (\pm 0.0050)$ (using average A_T - C_T data). Over 15 years, both results lead to a trend of between $-0.0154.\text{decade}^{-1}$ and $-0.016.\text{decade}^{-1}$ (Table 3). Given all uncertainties attached to pH calculations, our estimates either based on $f\text{CO}_2$ (and reconstructed A_T) or A_T - C_T observations show that acidification occurred in the Mozambique Channel at a rate similar to that reported for the northern subtropics (-0.017 .

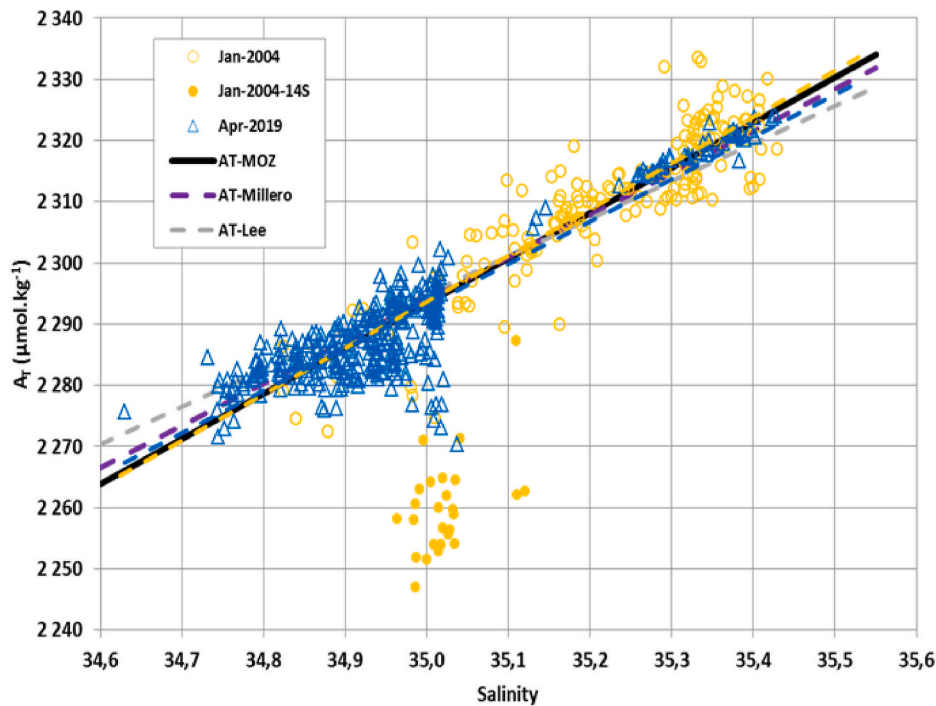


Fig. 5. Total Alkalinity (A_T , $\mu\text{mol.kg}^{-1}$) versus salinity in surface water in the Mozambique Channel ($14\text{--}25^\circ\text{S}$) observed in January 2004 (orange circles) and April 2019 (blue triangle). Linear relation for each period are also shown (orange and blue dashed-lines). In January 2004 data north of 14°S near Mayotte are identified with filled orange circles and not used for the A_T /SSS relationship. Also shown are the A_T /SSS relationships from Millero et al. (1998) for the Indian Ocean (Purple dashed) and from Lee et al. (2006) for the subtropical oceans (Grey dashed). The A_T /SSS relationship based on Jan-2004 and Apr-2019 data in the Mozambique Channel (noted AT-MOZ, black line) is the final relationship used in this analysis: $A_T = 73.841 * S - 291.02$.

Table 3

Mean sea surface and trends of pH in the band $14^\circ\text{S}\text{--}25^\circ\text{S}$ in May 1963, January 2004 and April 2019 in the Mozambique Channel. Nb is the number of data (ND= No Data). Standard deviations for mean values and errors for trends are indicated in bracket. Errors for trends are based on $f\text{CO}_2$, A_T and C_T measurements uncertainty for each cruise as documented in the main text and Table S1 in Supplementary Material. pH is calculated with $f\text{CO}_2$ data and A_T /SSS relationship or with measured C_T and A_T (for 2004 and 2019). Averaged pH at SST-29 °C is also listed. Adjusted values for April 2004 and April 1963 as specified were used to estimate the trends of pH for different periods. Last line is the pH trend without the long-term warming of $+0.011\text{ }^\circ\text{C.yr}^{-1}$.

Period	Nb	pH	pH-29C	Nb	pH	pH-29C
	($f\text{CO}_2$)	TS	TS		(A_T - C_T)	TS
April-2019	1677	8.040 (0.008)	8.034 (0.007)	376	8.035 (0.008)	8.029 (0.008)
January-2004	480	8.039 (0.008)	8.045 (0.009)	142	8.044 (0.010)	8.051 (0.010)
May-1963	59	8.143 (0.008)	8.094 (0.015)	ND	ND	ND
April-2004 (adjusted)			8.063		8.059	
Avril-1963 (adjusted)			8.126		ND	
Trend		pH ($f\text{CO}_2$) TS.yr $^{-1}$			pH (A_T - C_T) TS.yr $^{-1}$	
2004–2019		–0.00154 (0.00100)			–0.00160 (0.00149)	
1963–2004		–0.00154 (0.00039)				
1963–2019		–0.00154 (0.00028)				
1963–2019 (without warming)		–0.00137 (0.00028)				

decade $^{-1}$, e.g. Bates et al., 2014; Ono et al., 2019). This is, however, much lower than previous estimates of pH trends derived from $f\text{CO}_2$ data at large scale in the Indian Ocean. Lauvset et al. (2015) report rates between $-0.024\text{.decade}^{-1}$ for the period 1981–2011 and -0.027 .

decade $^{-1}$ for 1991–2011 which suggests a faster pH decrease in the Indian Ocean compared to other regions. The pH trend of -0.00160.yr^{-1} (± 0.00149) derived in our observations in the Mozambique Channel between 2004 and 2019 is also close to the average trend of -0.00165.yr^{-1} (± 0.00038) computed over 2004–2019 in the same region from reconstructed monthly pH fields using a neural-network method (Denvil-Sommer et al., 2019; Chau et al., 2020).

The carbonate system parameters (A_T , C_T , $f\text{CO}_2$) measured in January 2004 and April 2019 described in this section, along with pH estimates using different inputs (A_T and C_T or $f\text{CO}_2$), show that (i) N- A_T concentrations are stable, (ii) there is a well characterized A_T /SSS relationship, (iii) the changes in C_T , $f\text{CO}_2$ and pH over 15 years are significant and (iv) when seasonality is taken into account the observed trends of C_T , $f\text{CO}_2$ and pH likely reflect the uptake of anthropogenic CO_2 . In the following section, we explore these signals over a longer time period extending back to the sixties.

3.2. Detecting the long-term trends of $f\text{CO}_2$ and pH in the Mozambique channel

3.2.1. Comparison with historical observations collected in the Mozambique channel in 1963

In order to explore the long-term change in $f\text{CO}_2$ and pH in the Mozambique Channel, we compared our $f\text{CO}_2$ observations obtained in 2004 and 2019 with the only other $f\text{CO}_2$ dataset obtained in this region along a latitudinal transect in May 1963 (Keeling and Waterman, 1968). To estimate pH changes, we used $f\text{CO}_2$, SST and SSS data for the 3 cruises and the A_T /SSS relation described above. We note that in May 1963, salinity was not measured and for this cruise we used the mean monthly salinity from the World Ocean Atlas, WOA (Antonov et al., 2006), as listed in the SOCAT data product (Bakker et al., 2016). The mean WOA salinity in the band $14^\circ\text{S}\text{--}25^\circ\text{S}$ in May is 34.88 close to those measured in January 2004 (35.15) and April 2019 (34.97). The use of WOA salinity has a negligible impact on pH calculations and derived trends. The comparison of observations obtained in 1963, 2004 and 2019 is presented in Fig. 7 for the original data and in Fig. 8 for $f\text{CO}_2$ and pH normalized at SST 29 °C along with calculated N- C_T for these cruises.

The atmospheric $x\text{CO}_2$ value in May 1963 was around 315 ppm, 90

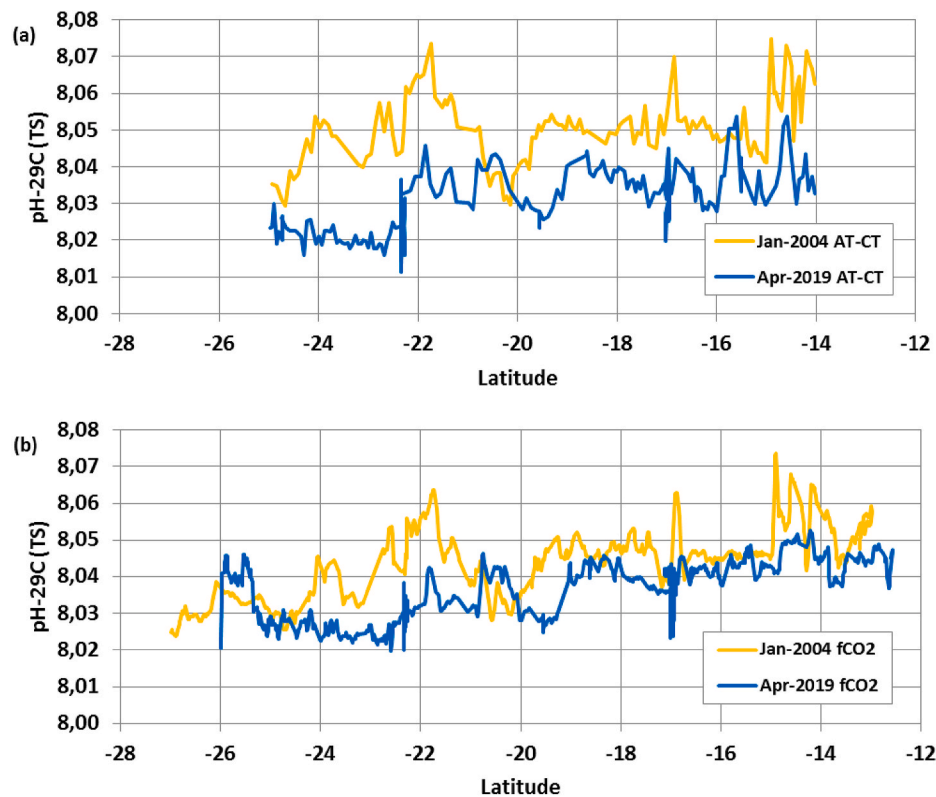


Fig. 6. Surface water pH (at SST 29 °C) distribution in the Mozambique Channel observed in January 2004 (orange) and April 2019 (blue). (a) pH at 29 °C calculated with A_T and C_T pairs. (b) pH at 29 °C calculated with fCO_2 and A_T reconstructed from salinity. Data very close to Islands filtered (e.g. Juan de Nova at 17°S).

ppm lower than in 2019. Like in April 2019, oceanic fCO_2 in May 1963 was quite homogeneous in the Mozambique Channel increasing progressively northward with values ranging from 290 μatm at 25°S to 305 μatm at 16°S (Fig. 7b). This region was a small CO_2 sink during this period. Average ΔfCO_2 was $-9.3 (\pm 4.9) \mu atm$ in May 1963, very close to the climatological value for May ($-5.3 \pm 7.4 \mu atm$ for a reference year 2000, Takahashi et al., 2009) and not very different from our recent observations in April 2019 (near equilibrium with average ΔfCO_2 of $+2.5 \pm 7.9 \mu atm$). The most remarkable change is, like for atmospheric CO_2 , the much lower ocean fCO_2 observed in May 1963 (Fig. 7b, Table 2). Consequently this leads to higher pH in 1963 compared to 2004 or 2019 (Fig. 7c, Table 3). Based on these data, oceanic fCO_2 increased by $+101 (\pm 5) \mu atm$ from 1963 to 2019 and pH decreased by $-0.104 (\pm 0.006)$. This change in pH is similar to the reduction estimated for the global ocean between preindustrial and modern times of -0.11 (Jiang et al., 2019). These differences are a snapshot between two cruises conducted 56 years apart and modulated by SST variations that should be taken into account to better interpret the long-term trends of fCO_2 and pH.

3.2.2. Seasonal temperature and the impact of long-term warming on the fCO_2 trend

The observed SST seasonal variation is significant with the ocean being much colder in May 1963 compared to January 2004 or April 2019 (Fig. 7a). The measurements in 1963 present also a sharp front in SST at 20°S which is not seen in fCO_2 records (Fig. 7b). This is probably because both A_T and C_T concentrations in May 1963 (not measured in 1963) drive fCO_2 the same way as observed in April 2019 (see description above, Fig. 2). In 1963, the increase in SST from 24 °C in the south to 27 °C in the north would lead to a fCO_2 increase of about $+45 \mu atm$ but measurements show only a difference of $+15 \mu atm$ from south to north. This suggests a competitive balance between the thermal, physical and biological processes, all leading to rather homogeneous fCO_2 and pH distributions in 1963 (Fig. 7b and c).

In addition, the Indian Ocean, including the Mozambique Channel, experienced a significant long-term warming in recent decades that would drive part of the fCO_2 and pH trends. Based on monthly SST products (Reynolds et al., 2002) extracted at 15°S–20°S in the Mozambique Channel from 1981 to 2019 we estimated an annual long-term warming of $+0.011 (\pm 0.007) ^\circ C.yr^{-1}$ (Supp. Fig. S11). Such a pronounced warming has also been identified in the Indian Ocean subtropics ($>0.1 ^\circ C.decade^{-1}$) dating back to the sixties (Alory et al., 2007; Roxy et al., 2014). It could be due to a fast response to recent climate change or to natural multi-decadal variability (Zinke et al., 2014). Relying on corals sampled in the reefs off Southwestern Madagascar at 43°E–23°S, Zinke et al. (2014) reconstructed a warming rate of $+0.13 ^\circ C.decade^{-1}$ between the years 1720 and 1800 and between 1900 to present.

A long-term warming around $+0.1 ^\circ C.decade^{-1}$ is also consistent with the observed SST in May 1963 in the band 14°S–20°S ($26.82 \pm 0.25 ^\circ C$) being $0.7 ^\circ C$ lower than the mean climatological SST in May computed in recent years ($27.52 \pm 0.39 ^\circ C$ for the period 2000–2018). This long-term warming would increase sea surface fCO_2 by about $+7.5 \mu atm$ and would decrease pH by -0.009 units, a signal not directly linked to the oceanic CO_2 uptake. This corresponds to about 7% of the net fCO_2 increase of $+101 \mu atm$ observed between 1963 and 2019.

3.2.3. Changes in fCO_2 , pH and C_T in the Mozambique channel over 56 years

To separate the effect of temperature and anthropogenic CO_2 , fCO_2 and pH were normalized at SST 29 °C (Fig. 8a and b). We also compared $N-C_T$ calculated with fCO_2 and reconstructed A_T for the 3 cruises (Fig. 8c, Table 2). To validate the pH and $N-C_T$ calculations based on fCO_2 data for 1963, we first compared the $N-C_T$ calculated with fCO_2 ($N-C_{Tcal}$) and reconstructed A_T with $N-C_T$ derived from the measurements ($N-C_{Tmes}$) described in Section 3.1 for 2004 and 2019. On average and taking into account the uncertainty of the measurements and calculations, the $N-C_{Tcal}$ and $N-C_{Tmes}$ values were of the same order for each cruise

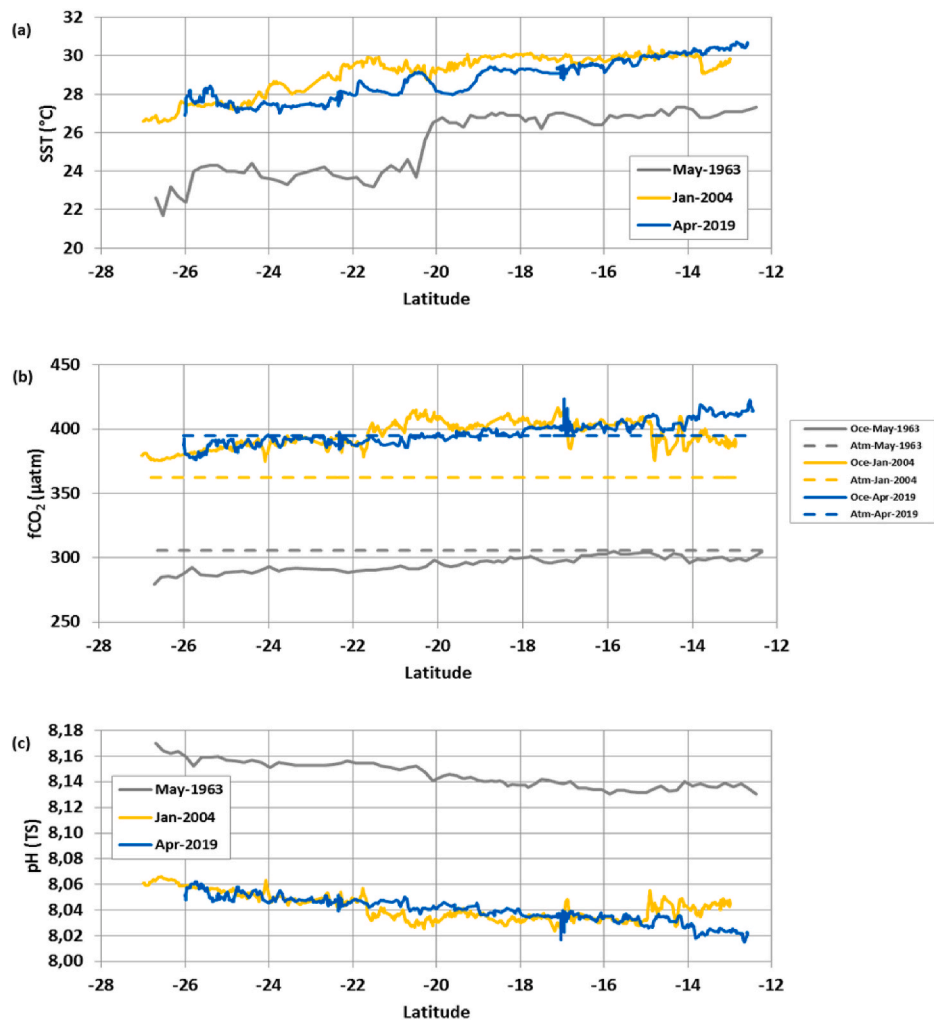


Fig. 7. Surface water temperature (a), $f\text{CO}_2$ (b) and calculated pH (c) in the Mozambique Channel observed in May 1963 (grey), January 2004 (orange) and April 2019 (blue). In (b) atmospheric $f\text{CO}_2$ also shown for each year (same color, dashed line).

(Table 2). In 2019 both $N\text{-C}_{\text{Tcal}}$ and $N\text{-C}_{\text{Tmes}}$ were higher than in 2004 (respectively +7 and +12 $\mu\text{mol kg}^{-1}$) and adjusted values for April lead to the same $N\text{-C}_T$ trend for 2004–2019 (Table 2). We have thus confidence in $N\text{-C}_T$ and pH values calculated with $f\text{CO}_2$ and the A_T/SSS for 1963.

For all three cruises, $f\text{CO}_2$ -29C and $N\text{-C}_T$ decreased northward and the opposite for pH-29C (Fig. 8). In May 1963 the decrease occurred more sharply at the SST front near 20°S (Fig. 7a). Consequently, the changes in $f\text{CO}_2$, pH and $N\text{-C}_T$ between 1963 and 2004/2019 are slightly more pronounced in the North. The same contrast is observed for aragonite (Ω_{Ar}) and calcite (Ω_{Ca}) saturation states calculated with $f\text{CO}_2$ and A_T/SSS for each cruise (Supp. Fig. S12).

On average $f\text{CO}_2$ and $N\text{-C}_T$ in 1963 were much lower than in 2004 and 2019, and pH-29C much higher (Fig. 8, Tables 2 and 3). To estimate the long-term trend, $f\text{CO}_2$ observations in May 1963 were adjusted to April 1963 (+11.9 μatm based on the climatology) and compared with April 2004 and 2019 to calculate the trends (Tables 2 and 3). From 1963 to 2004, the $f\text{CO}_2$, $N\text{-C}_T$ and pH trends were respectively +1.5 (± 0.3) $\mu\text{atm.yr}^{-1}$, +1.0 (± 0.4) $\mu\text{mol.kg}^{-1}.\text{yr}^{-1}$ and -0.0015 yr^{-1} (± 0.0004). From 1963 to 2019 results are almost the same, +1.6 (± 0.2) $\mu\text{atm.yr}^{-1}$, +1.0 (± 0.3) $\mu\text{mol.kg}^{-1}.\text{yr}^{-1}$ and -0.0015 yr^{-1} (± 0.0003).

These results, although based on only three cruises, are remarkably close to the atmospheric $x\text{CO}_2$ trend of +1.6 ppm.yr^{-1} over 1963–2019 and to theoretical trends of +1.04 $\mu\text{mol kg}^{-1}.\text{yr}^{-1}$ for C_T and -0.00165 yr^{-1} for pH assuming that the ocean followed the atmospheric CO_2

increase and constant alkalinity. Subtracting the effect of the long-term warming in this region (+0.011 $^\circ\text{C.yr}^{-1}$) on the $f\text{CO}_2$ trend (+0.13 $\mu\text{atm.yr}^{-1}$), leads to a trend of $f\text{CO}_2$ of 1.39 $\mu\text{atm.yr}^{-1}$ (1963–2004) or 1.44 $\mu\text{atm.yr}^{-1}$ (1963–2019) that would reflect the anthropogenic CO_2 uptake. Our results also suggest that observed trends in the Mozambique Channel were slightly more pronounced in the recent decades (Tables 2 and 3), but this is deduced from only three cruises. For a better evaluation of the decadal variability and long-term trends we now focus on the southern region of the Mozambique Channel where more $f\text{CO}_2$ data are available for different seasons and years (Table 1).

3.3. Long-term trends in the southern region of the Mozambique channel

To confirm the changes observed in the Mozambique Channel from the three cruises in 1963, 2004 and 2019, we explored the $f\text{CO}_2$ and pH variations based on all data available in SOCAT-v2020 around 25°S. Here we selected the data in the region 23.5°S–26.5°S/38°E–42°E (identified with a green circle in Fig. 1). This added 3 cruises conducted in June 1995, December 2003 and July 2014 (Table 1). In 1995 and 2003 C_T and A_T were also measured at fixed stations (Sabine et al., 1999; Murata et al., 2010) and we used these surface data (3–10m) to compare with $N\text{-C}_T$ calculated from $f\text{CO}_2$ and A_T .

Sea surface temperature, $f\text{CO}_2$ and pH (calculated) for the six cruises are shown in Fig. 9 and the averages of observed and calculated properties around 25°S for each cruise are listed in Table 4. For each period

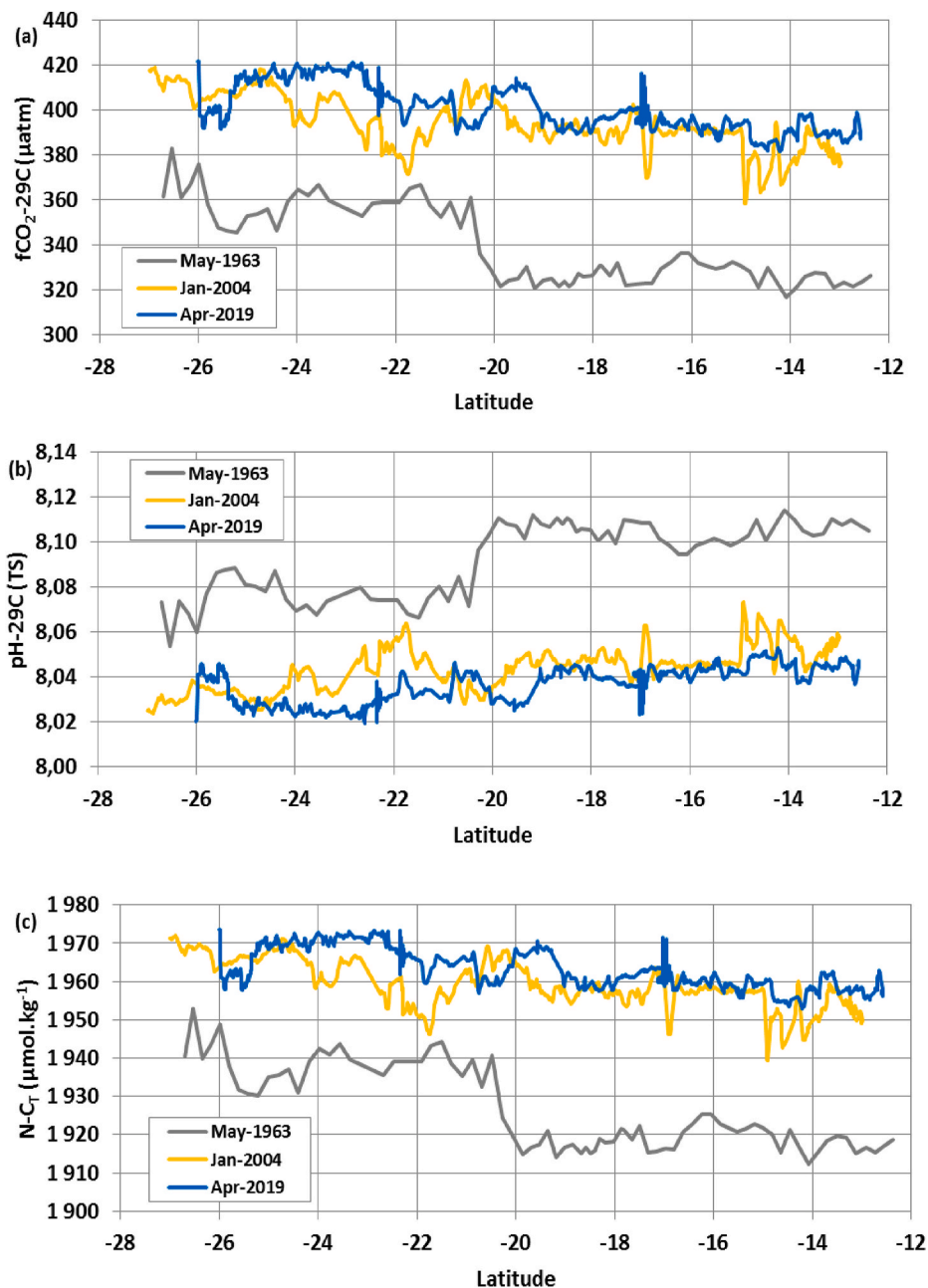


Fig. 8. Surface water $f\text{CO}_2$ at $\text{SST} = 29^\circ\text{C}$ (a) and calculated pH at $\text{SST} = 29^\circ\text{C}$ (b) in the Mozambique Channel observed in May 1963 (grey), January 2004 (orange) and April 2019 (blue). In (c) also shown N-C_T distribution calculated with $f\text{CO}_2$ and A_T reconstructed.

SST , $f\text{CO}_2$ and pH are fairly homogeneous in this region (Fig. 9) and this translates into a low standard-deviations around the mean (Table 4). The ocean was colder in May, June and July than in December, January and April (Fig. 9a). For the cold season as expected, the $f\text{CO}_2$ was the lowest in May 1963 ($<300 \mu\text{atm}$) compared to June 1995 ($>300 \mu\text{atm}$) and July 2014 ($>350 \mu\text{atm}$) and pH was higher in 1963 (>8.15) compared to 2014 (<8.09). During the warm season (December–April), $f\text{CO}_2$ was always higher than $370 \mu\text{atm}$ (Fig. 9b). As described above, the same $f\text{CO}_2$ values (near $390 \mu\text{atm}$) were observed in January 2004 and April 2019, i.e. 15 years apart. The lowest pH (range $8.033 < \text{pH} < 8.066$) was always observed during the warm season (Fig. 9c).

The two cruises conducted one month apart in December 2003 and January 2004 on different ships recorded surprisingly the same range of $f\text{CO}_2$, around $385\text{--}390 \mu\text{atm}$ (Table 4). At 40°E , however, despite SST being the same (Fig. 9a), $f\text{CO}_2$ was higher in December 2003 than in January 2004 by $+12 \mu\text{atm}$ on average (Fig. 9b). This is opposed to the

climatology according to which December $f\text{CO}_2$ is generally lower by $-20 \mu\text{atm}$ than January in this region (Supp. Fig. S6). An inspection of the Quality Control information available on-line in SOCAT (www.socat.info) indicated that for the December 2003 cruise (Expocode 49NZ20031209) there was no equilibrator temperature and pressure recorded. We are thus less confident with the accuracy of $f\text{CO}_2$ data for this cruise (Lauvset et al., 2019). Like for our cruises in 2004 and 2019, the C_T concentrations measured in 1995 and 2003 were close to the C_T calculated from $f\text{CO}_2$ and our A_T/SSS relationship (last two columns in Table 4) confirming the pH values calculated the same way for different years and seasons. For the trend analysis we thus use pH and C_T calculated using $f\text{CO}_2$ data for all cruises (except December 2003).

The temporal evolutions of $f\text{CO}_2$, pH and N-C_T averaged at 25°S are shown in Fig. 10 and the trends evaluated on different periods listed in Table 5 and illustrated in Fig. 11. The trends were estimated after adjusting $f\text{CO}_2$ data to June each year (grey diamonds in Fig. 10). We

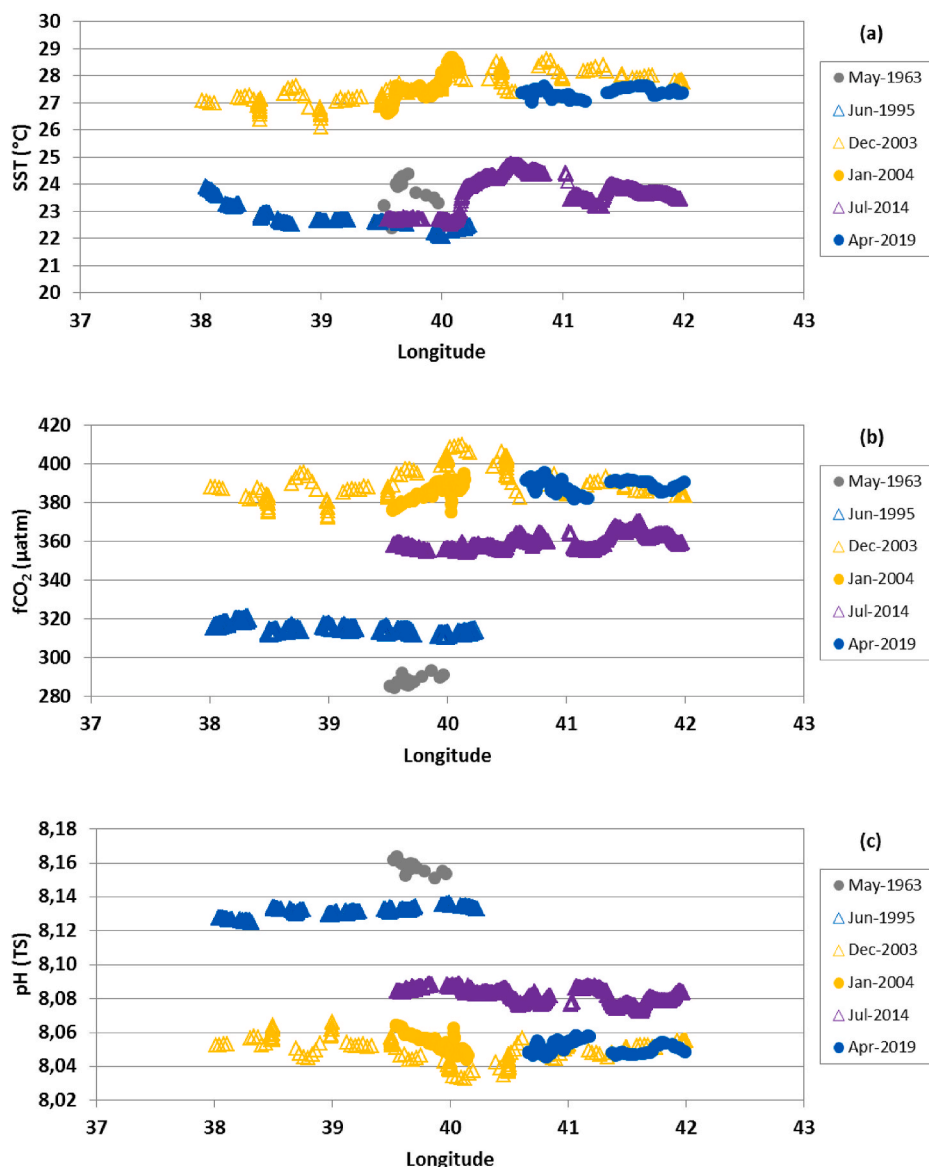


Fig. 9. Sea surface water temperature (a), fCO_2 (b) and calculated pH (c) around 25°S in the Mozambique Channel observed in May 1963, June 1995, December 2003, January 2004, July 2014 and April 2019. Cruises are listed in Table 1 and tracks identified in Fig. 1. The mean observations for each cruise are listed in Table 4.

Table 4

Mean sea surface measured or calculated properties around 25°S for 6 cruises in the south part of Mozambique Channel. Nb = number of data from surface underway sampling used to calculate $[H^+]$, pH and $N-C_T$. Standard deviations are in bracket. $N-C_T$ stands for salinity normalized C_T concentrations either calculated with fCO_2 and A_T ($N-C_{Tcal}$) or measured ($N-C_{Tmes}$) when available. ND= No Data.

Period	Nb	SST °C	fCO_2 µatm	$[H^+]$ nmol.kg ⁻¹	pH TS	$N-C_{Tcal}$ µmol.kg ⁻¹	$N-C_{Tmes}$ µmol.kg ⁻¹
May-1963	15	23.70 (0.59)	288.6 (2.6)	6.965 (0.055)	8.157 (0.003)	1937.8 (5.6)	ND
June-1995	717	22.66 (0.39)	314.6 (1.9)	7.381 (0.044)	8.132 (0.003)	1964.7 (2.6)	1961.3 (4.8) n9
Dec-2003	180	27.58 (0.53)	389.3 (8.1)	8.901 (0.146)	8.051 (0.007)	1968.4 (3.9)	1967.4 (5.3) n5
Jan-2004	111	27.61 (0.53)	384.6 (4.5)	8.813 (0.101)	8.055 (0.005)	1965.6 (3.3)	1960.5 (4.5) n24
Jul-2014	820	23.57 (0.67)	359.7 (3.9)	8.268 (0.080)	8.083 (0.004)	1985.9 (5.0)	ND
Apr-2019	156	27.31 (0.16)	387.8 (3.8)	8.864 (0.080)	8.052 (0.004)	1969.9 (1.4)	1972.6 (2.0) n17

also compared the observational results with the pCO_2 and pH values reconstructed by Chau et al. (2020). Here we extracted the CMEMS-LSCE-NN model gridded results at the location 25°S-40°E. The trends from the model are evaluated for June to compare with observations (Fig. 12) or using the annual values (Table 5). Given the errors in the trends estimated for each property based on both measurements

uncertainty, spatial variability and pH or $N-C_T$ calculations, trends for short periods, e.g. 1995–2004 (Fig. 11) have large errors and thus the interpretation of observed changes is mainly limited to multi-decadal variations (1963–1995 versus 1995–2019).

We first noted that the long-term trends estimated with all data at 25°S are almost identical to those derived when using only 1963 and

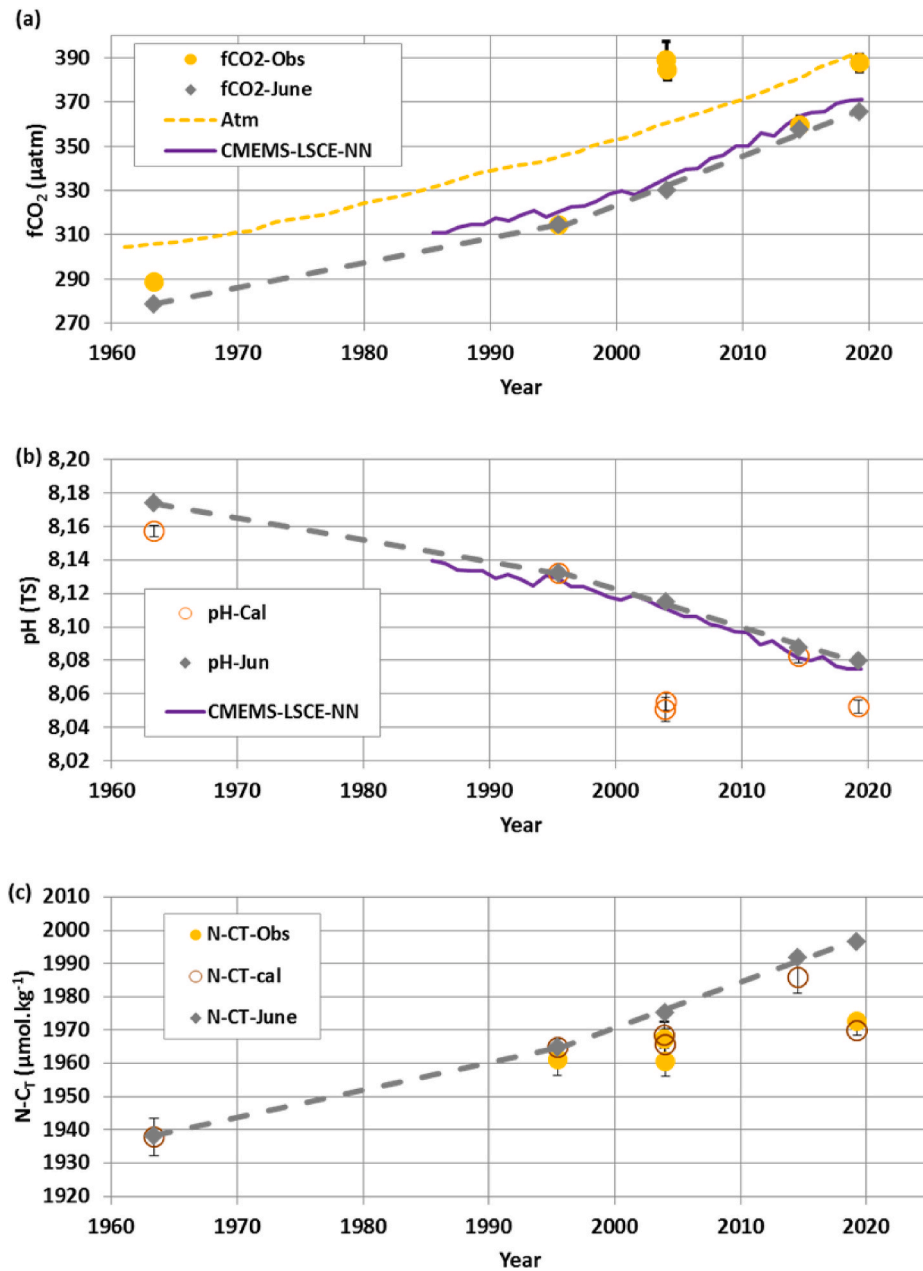


Fig. 10. Temporal evolution of $f\text{CO}_2$ (a), pH (b) and N-C_T (c) around 25°S in the Mozambique Channel based on data shown in Fig. 9. Measured $f\text{CO}_2$ and N-C_T are indicated by orange dots. pH and N-C_T calculated with $f\text{CO}_2$ and A_T are indicated by open circles. In all panels, values adjusted to the month of June indicated by grey diamond and used for trend estimates (dashed grey lines). In (a) and (b) results from monthly reconstructed $p\text{CO}_2$ and pH (at 25°S – 40°E) shown in purple line for June 1985–2019 (CMEMS-LSCE-NN, Chau et al., 2020). In (a) also shown the atmospheric $f\text{CO}_2$ (orange dotted line). The mean observations for each cruise are listed in Table 4 and trends listed in Table 5. Standard-deviations for observations and calculated pH or N-C_T are indicated by vertical bars (generally about the size of symbols).

2019 observations in the Mozambique Channel for the band 14°S – 25°S as described above. This suggests that the results at 25°S reflect the trends in a larger domain. However, these additional data allowed us to identify a shift in the trends before and after 1995, as expected from the recent faster increase of atmospheric CO_2 concentrations. At 25°S , the trends evaluated over the period 1995–2019 were almost twice as large as those evaluated over 1963–1995 (Table 5, Fig. 11). For $f\text{CO}_2$ we estimated an annual rate that changed from $+1.14 (\pm 0.23) \mu\text{atm.yr}^{-1}$ in 1963–1995 to $+2.20 (\pm 0.26) \mu\text{atm.yr}^{-1}$ in 1995–2019 (Figs. 10a and 11). For pH the trends varied from $-0.00129 (\pm 0.00042)$ to $-0.00227 (\pm 0.00048)$ unit yr^{-1} for the same periods (Figs. 10b and 11). To confirm these results we also evaluated the temporal change of pH based on $[\text{H}^+]$ concentrations calculated for each cruise (Supp. Fig. S13) and using Equation (3) (Kwiatkowski and Orr, 2018).

$$\Delta\text{pH} = -1 \Delta[\text{H}^+]/2.303 [\text{H}^+] \quad (3)$$

where ΔpH and $\Delta[\text{H}^+]$ are the temporal differences between each period (1995 versus 1963 or 2019 versus 1995) and $[\text{H}^+]$ the concentration at

the beginning of each period (1963 or 1995). The derived pH trends using Equation (3) are -0.00137 yr^{-1} for 1963–1995 and -0.00232 yr^{-1} for 1995–2019 (Table 5). Like for the trends deduced from the mean pH values at 25°S (Fig. 10b), the pH trend based on $[\text{H}^+]$ concentrations is about twice faster in 1995–2019. For the recent period the observed $f\text{CO}_2$ and pH trends are remarkably close to those derived from the CMEMS-LSCE-NN model (Fig. 10a and b, Fig. 12, Table 5). For C_T , we estimated a trend of $+0.82 (\pm 0.41) \mu\text{mol.kg}^{-1}.\text{yr}^{-1}$ for 1963–1995 and $+1.37 (\pm 0.42) \mu\text{mol.kg}^{-1}.\text{yr}^{-1}$ for 1995–2019 in the same range as the trends deduced when comparing data collected in 2004 and 2019 in the whole Channel (section 3.1, Table 2) and indicative of the accumulation of anthropogenic CO_2 .

3.4. Anthropogenic CO_2 in the southern region of the Mozambique channel

In order to separate the contributions of natural or climate change induced variations (e.g. warming) and the accumulation of

Table 5

Trends observed around 25°S in the Mozambique Channel evaluated from observations between 1963 and 2019 adjusted to June (as shown in Fig. 10 and Supp. Fig. S13 for $[H^+]$). Standard errors of slope are in bracket. Trends for pH are also calculated from $[H^+]$ concentrations following Equation (3) (see text, noted pH_{H^+}). Also indicated are the trends for atmospheric xCO_2 for different periods and from the monthly reconstructed pCO_2 and pH values based on a neural network model (CMEMS-LSCE-NN, Denvil-Sommer et al., 2019; Chau et al., 2020). For CMEMS-LSCE-NN the trends are for June or using all months in 1985–2019. For comparison the trends in June for period 1995–2004, 2004–2019 and 1995–2019 are underlined. ND = No Data. Detail for errors on the trends is documented in the Methods and Table S2 in the Supplementary Material.

Period	Atm xCO_2 ppm.yr ⁻¹	fCO_2 $\mu atm.yr^{-1}$	$[H^+]$ nmol.kg ⁻¹ .yr ⁻¹	pH_{H^+} TS.yr ⁻¹	pH TS.yr ⁻¹	$N-C_{Treal}$ $\mu mol.kg^{-1}.yr^{-1}$
1963–2019	+1.60 (0.02)	+1.55 (0.11)	0.0290 (0.0036)	−0.00188	−0.00167 (0.0002)	+1.04 (0.21)
1963–1995	+1.35 (0.02)	+1.14 (0.23)	0.0213 (0.0069)	−0.00137	−0.00129 (0.00042)	+0.82 (0.41)
<u>1995–2004</u>	+1.82 (0.04)	<u>+1.70</u> (0.81)	0.0318 (0.0242)	−0.00190	<u>−0.00185</u> (0.00144)	+1.15 (1.25)
<u>2004–2019</u>	+2.13 (0.04)	<u>+2.41</u> (0.43)	0.0452 (0.0145)	−0.00247	<u>−0.00243</u> (0.00079)	+1.46 (0.69)
<u>1995–2019</u>	+2.04 (0.03)	<u>+2.20</u> (0.26)	0.0412 (0.0085)	−0.00232	<u>−0.00227</u> (0.00048)	+1.37 (0.42)
CMEMS-LSCE-NN		fCO_2 $\mu atm.yr^{-1}$			pH TS.yr ⁻¹	
<u>1995–2004 June</u>		<u>+1.70</u> (0.95)			<u>−0.00186</u> (0.00163)	
<u>2004–2019 June</u>		<u>+2.45</u> (0.51)			<u>−0.00247</u> (0.00078)	
<u>1995–2019 June</u>		<u>+2.28</u> (0.23)			<u>−0.00234</u> (0.00039)	
1985–2019 June		+1.89 (0.14)			−0.00196 (0.00024)	
1995–2004 Annual		+2.02 (0.48)			−0.00203 (0.00071)	
1995–2019 Annual		+1.88 (0.14)			−0.00180 (0.00019)	
2004–2019 Annual		+1.80 (0.30)			−0.00165 (0.00038)	
1985–2019 Annual		+1.80 (0.09)			−0.00177 (0.00012)	

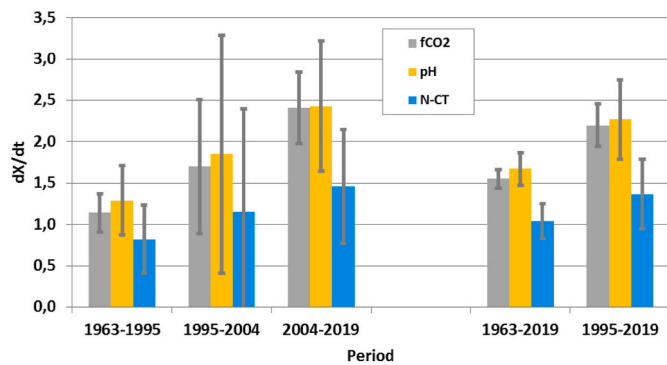


Fig. 11. Annual trends (see Table 5) estimated for different periods in the southern Mozambique Channel (25°S) based on observations for fCO_2 (grey, $\mu atm.yr^{-1}$), pH (orange, unit.yr⁻¹) and $N-C_T$ (blue, $\mu mol.kg^{-1}.yr^{-1}$). For pH, the annual trend is multiplied by -1000 (a pH trend of 1.5 in the figure is $-0.0015 yr^{-1}$). For short periods such as 1995–2004 the errors are large and thus the interpretation is limited. For longer periods, fCO_2 and pH trends are higher in 2004–2019 compared to 1963–1995 and mainly linked to anthropogenic CO_2 as suggested by $N-C_T$ changes.

anthropogenic CO_2 to the fCO_2 and pH trends described above, we evaluated the anthropogenic fraction of C_T (hereafter noted C_{ant}) in the southern Mozambique Channel region based on water-column observations. Data from two cruises at 25°S in June 1995 and December 2003 are available in the GLODAPv2.2019 data product (Olsen et al., 2019). Murata et al. (2010) used these observations to evaluate the changes of anthropogenic CO_2 concentrations in the interior of the South Indian Ocean. They estimated a mean increase of C_{ant} of $+7.9 (\pm 1.1) \mu mol.kg^{-1}$ from June 1995 to December 2003 in the upper layer of the subtropical water in the Central Indian Ocean. Over 8.5 years this corresponds to a trend of $+0.93 (\pm 0.13) \mu mol.kg^{-1}.yr^{-1}$, in the range of our estimate based on surface observations (Fig. 10c, Table 5). Specifically for the period 1995–2004, we evaluated an increase in $N-C_T$ of $+10.5 \mu mol.kg^{-1}$ in surface waters but over only 9 years the trend is uncertain, $+1.15 (\pm 1.25) \mu mol.kg^{-1}.yr^{-1}$ (Table 5).

To further explore C_T and C_{ant} variations across the Mozambique Channel, we revisited the data used by Murata et al. (2010) focusing on the stations within the same region as selected for surface data described in the previous section (25°S/38°E–42°E). To calculate C_{ant} we used the

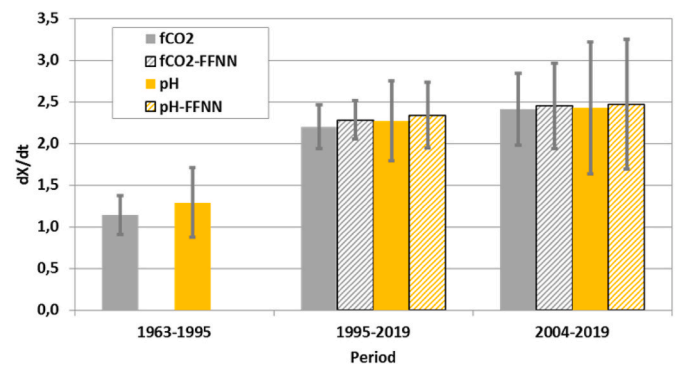


Fig. 12. Annual trends (see Table 5) for fCO_2 (grey, $\mu atm.yr^{-1}$) and pH (orange, unit.yr⁻¹) estimated for different periods in the southern Mozambique Channel (25°S) based on observations (filled bars) and the CMEMS-LSCE-FFNN model (hatched bars). For pH, the trend is multiplied by -1000 (a pH trend of 1.5 in the figure is $-0.0015 yr^{-1}$). Given the errors associated to these estimates, the trends are the same either based on observations or the CMEMS-LSCE-FFNN model.

TrOCA method developed by Touratier et al. (2007) (see Section 2.3). Because indirect methods like TrOCA are not suitable to evaluate C_{ant} concentrations in surface waters (due to biological activity and gas exchange) we calculated C_{ant} in the layer 150–200m below the nitracline. The averages of observed and calculated properties in this layer are listed in Table 6 as well as the differences between the cruises. From 1995 to 2003 C_T and $N-C_T$ increased by about $10 \mu mol.kg^{-1}$ and no significant change was observed for A_T . Our C_{ant} estimate in this region increased from $35.1 (\pm 1.2) \mu mol.kg^{-1}$ in 1995 to $42.3 (\pm 3.2) \mu mol.kg^{-1}$ in 2003. The C_{ant} increase of $+7.3 (\pm 3.4) \mu mol.kg^{-1}$ reported here around 25°S is very close to the average value of $+7.9 (\pm 1.1) \mu mol.kg^{-1}$ derived by Murata et al. (2010) in the subtropical Indian Ocean subsurface waters. The C_{ant} increase explains 70% of the C_T increase of $+10.5 \mu mol.kg^{-1}$ over this period (1995–2003). The remaining 30% is probably linked to natural C_T variations associated to internal processes such as eddy activity around 24°S (Swart et al., 2010) and/or remineralization as revealed by the decrease in oxygen concentration (Table 6).

Our estimate of C_{ant} variations at regional scale can be also compared to the results by Gruber et al. (2019a) who evaluated the changes in C_{ant} in the global ocean between 1994 and 2007. We extracted the C_{ant} data

Table 6

Mean observed or calculated properties and their temporal differences in the layer 150–200m in the region 25°S/38–42°E. Data are from GLODAPv2.2019 (Olsen et al., 2019). All units in $\mu\text{mol.kg}^{-1}$. Standard-deviations are in bracket. Nb is number of samples in the 150–200m layer.

Month-Year	Expocode	C_T	$N-C_T$	A_T	$N-A_T$	O_2	C_{ant}	Nb
Jun-1995	316N19950611	2070.8 (5.9)	2039.0 (5.2)	2329.8 (2.6)	2293.8 (1.9)	194.8 (11.8)	35.1 (1.2)	9
Dec-2003	49NZ20031209	2081.3 (14.2)	2048.0 (15.6)	2332.8 (5.6)	2295.5 (3.1)	184.4 (14.7)	42.3 (3.2)	8
Difference 2003–1995		+10.5 (15.4)	+9.0 (16.4)	+3 (6.7)	+1.6 (3.7)	−10.4 (18.9)	+7.3 (3.4)	

for the Mozambique Channel made available by Gruber et al. (2019b) and estimated the mean C_{ant} changes at 25°S in different layers (Table 7). The accumulation of C_{ant} between 1994 and 2007 is rather homogeneous in the Mozambique Channel (Supp. Fig. S14). In the top layer (0–200m) the mean C_{ant} increase between 1994 and 2007 is +14.03 (± 0.78) $\mu\text{mol.kg}^{-1}$ in the Channel (15°S–27°S). At 25°S, the accumulation in the layer 150–200m is +12.94 (± 0.56) $\mu\text{mol.kg}^{-1}$, i.e. a rate of +1.00 (± 0.04) $\mu\text{mol.kg}^{-1}.\text{yr}^{-1}$ which is slightly higher than our C_{ant} estimate of +0.86 (± 0.4) $\mu\text{mol.kg}^{-1}.\text{yr}^{-1}$ based on TrOCA and for the period June 1995 to December 2003.

Although the C_{ant} estimates described above were obtained for different periods and using different methods (Murata et al., 2010; Gruber et al., 2019a; this study), all results lead to the same conclusion: there was a gradual increase in C_T concentrations in the upper waters of the southern Mozambique Channel from +0.82 (± 0.41) $\mu\text{mol.kg}^{-1}.\text{yr}^{-1}$ in 1963–1995 to +1.37 (± 0.42) $\mu\text{mol.kg}^{-1}.\text{yr}^{-1}$ in 1995–2019 (Table 5, Fig. 11). It is mainly driven by the accumulation of anthropogenic CO_2 (Tables 6 and 7). This also explains the observed long-term trends of $f\text{CO}_2$ and the progressive pH decline in this region (Fig. 10). The warming of +0.11 $^{\circ}\text{C}.\text{decade}^{-1}$ would translate into a pH decrease of $-0.0017.\text{decade}^{-1}$, i.e. about 10% of the observed long-term trend for 1963–2019 of $-0.0167 (\pm 0.002).\text{decade}^{-1}$. Most of the observed pH change in the Mozambique Channel is thus likely due to anthropogenic CO_2 . This could impact not only the biological processes in the open ocean but also coral reef ecosystems in this region.

3.5. A Paleo-acidification perspective

Like in other regions, coral reefs in the Mozambique Channel are subject to multiple stressors due to warming, sea level rise and acidification, combined or not to local anthropization (e.g. in Mayotte). Historical SST and pH can be reconstructed from aragonite skeletal cores collected from massive scleractinian coral species like *Porites* sp. from geochemical proxies such as trace element ratios (e.g. Li/Mg, Sr/Ca), oxygen ($\delta^{18}\text{O}$) or boron ($\delta^{11}\text{B}$) isotopic ratio (e.g. Montagna et al., 2014; Tierney et al., 2015; Liu et al., 2014; Wu et al., 2018; D’Olivo et al., 2019; Cuny-Guirriec et al., 2019). Above we have estimated the change in pH since 1963. If we assume that the trends derived from observations between the sixties and 2019 are representative of the trend over the historical period (i.e. $f\text{CO}_2$ tracks atmospheric CO_2) historical changes in sea surface $f\text{CO}_2$, pH and $N-C_T$ can be evaluated back to the pre-industrial period (Fig. 13a and b). We used historical atmospheric $x\text{CO}_2$ data for the southern hemisphere reconstructed by Meinshausen et al. (2017) for the period 1800–2014 along with recent atmospheric $x\text{CO}_2$ recorded over 2015–2019 (Dlugokencky and Tans, 2020). C_T and

Table 7

Mean C_{ant} accumulation and trends between 1994 and 2007 in the region 25°S/42°E in different layers (data from Gruber et al., 2019b). Standard-deviations are in bracket.

Layer	Delta- C_{ant}	Trend (1994–2007)
	$\mu\text{mol.kg}^{-1}$	$\mu\text{mol.kg}^{-1}.\text{yr}^{-1}$
0–30m	14.44 (0.05)	1.11 (0.004)
50–100m	14.04 (0.19)	1.08 (0.015)
100–150m	13.64 (0.15)	1.05 (0.012)
150–200m	12.94 (0.56)	1.00 (0.043)

pH were calculated assuming constant salinity (35) and alkalinity (2300 $\mu\text{mol.kg}^{-1}$, the mean of all A_T observations in January 2004 and April 2019 was $2297.6 \pm 14.7 \mu\text{mol.kg}^{-1}$, Fig. 3a). We also assume that the oceanic $f\text{CO}_2$ is either in equilibrium with the atmosphere (orange line in Fig. 13a and b) or that $f\text{CO}_2$ seasonality is constant over time (grey lines in Fig. 13a and b).

The results of the reconstruction for the recent decades (Fig. 13a) show a good agreement with observations for $f\text{CO}_2$ and pH when available. For the period 1985–2019 the reconstructed $f\text{CO}_2$ and pH are also close to the monthly values from the neural network model (Chau et al., 2020, purple lines in Fig. 13a). Reconstructed $N-C_T$ concentrations are also in the range of $N-C_T$ measured or calculated between 1963 and 2019. In the year 1800, values of $f\text{CO}_2$, pH and $N-C_T$ were respectively around 270 (± 10) μatm , 8.18 (± 0.014) and 1915 (± 10) $\mu\text{mol.kg}^{-1}$. This gives a reference for pH reconstructions based on 2 m-long coral cores recently collected at different locations along the Mozambique Channel during the CLIM-EPARSES cruise (work in progress, Tribollet, 2019, 2020).

Since 1800, the mean annual pH decreased progressively from 8.180 to 8.136 in 1963 (the first direct observation) and then decreased sharply to reach 8.05 in 2019. The pH decline of -0.13 between 1800 and 2019, evaluated here at local scale, is slightly larger than the -0.11 pH units estimated for the global ocean (Jiang et al., 2019). Based on our reconstruction, we evaluated a pH trend of $-0.0027.\text{decade}^{-1}$ during 1800–1963, $-0.0138.\text{decade}^{-1}$ during 1963–1995 and $-0.0187.\text{decade}^{-1}$ during 1995–2019. Recalling our results based on observations (Table 5), it is clear that the rate of acidification has increased over the past recent decades, and it is likely that this process will continue in the next decade given the rapid increase of atmospheric CO_2 concentrations that reached a new record of +2.6 $\text{ppm}.\text{yr}^{-1}$ in 2019 for a non ENSO year (Dlugokencky and Tans, 2020). If future atmospheric CO_2 levels keep increasing at the same rate, a further decrease of pH by -0.1 is likely to occur by 2040 ($\text{pH} < 8$) while aragonite saturation state (Ω_{Ar}) would reach the value of 3 (Supp. Fig. S14) which is below the critical threshold of $\Omega_{\text{Ar}} = 3.25$ that seems to limit the distribution of tropical coral reefs in the contemporary ocean (e.g. Hoegh-Guldberg et al., 2007).

Such a rapid reduction of pH and Ω_{Ar} in the Mozambique Channel in response to anthropogenic CO_2 emissions could have severe negative impacts on coral reefs because of a simultaneous reduction of calcification of the main reef framebuilders (corals and crustose coralline algae; Pandolfi et al., 2011) and a stimulation of carbonate dissolution processes (Schönberg et al., 2017; Eyre et al., 2018; Tribollet et al., 2019). Impacts on coral reefs of combined effects of ocean warming and acidification, together with local disturbances (e.g. eutrophication), need to be further investigated as the interaction of stressors might be synergistic or antagonistic (Chauvin et al., 2011; Trnovsky et al., 2016; Schönberg et al., 2017; Boyd et al., 2018). Future studies need to address impacts of multiple drivers on coral reefs at the regional scale, f.i. along thermal, pH and pollution gradients, to better apprehend and predict the fate of those ecosystems.

4. Summary and concluding remarks

This study presents new observations of the carbonate system in the Mozambique Channel for January 2004 and April 2019. Remarkable

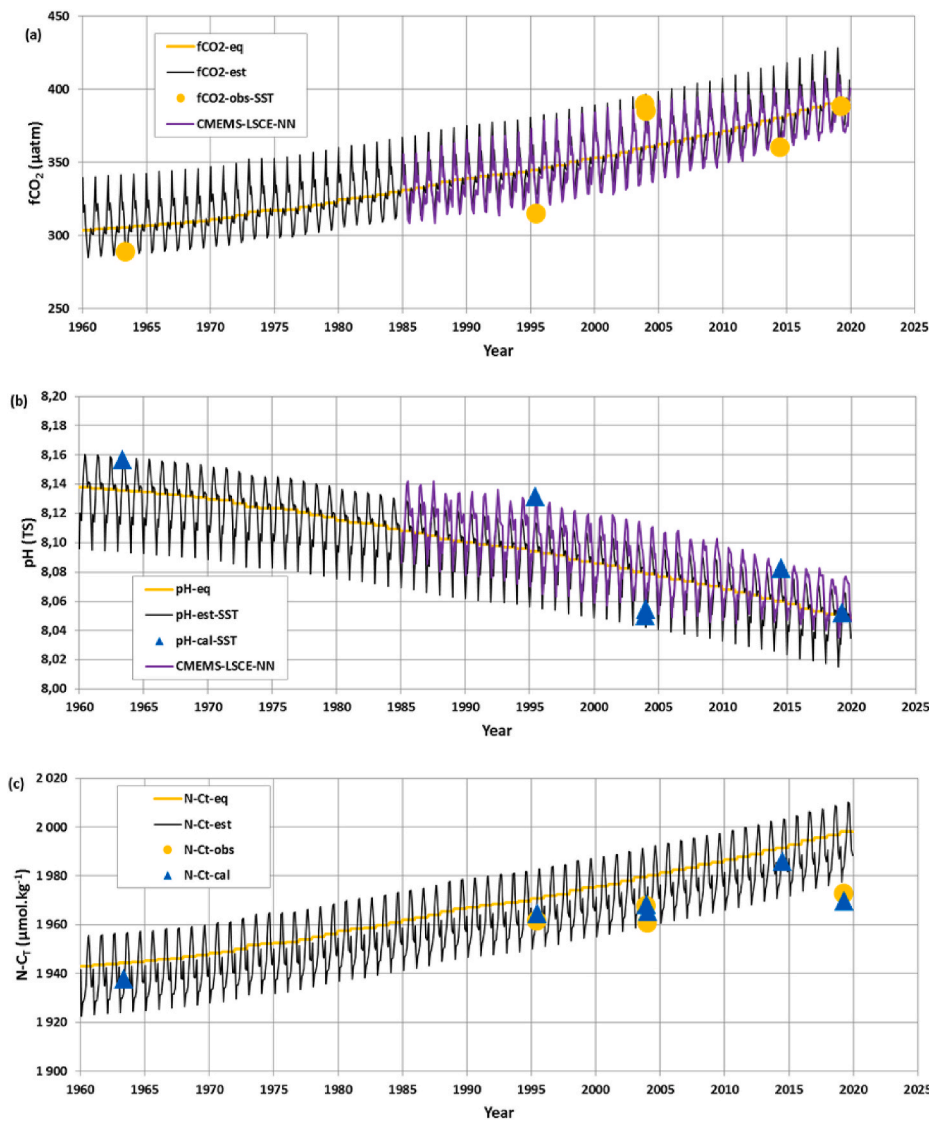


Fig. 13. a: Reconstructed (black lines) sea surface fCO₂ (a), pH (b) and N-C_T (c) for the periods 1960–2019 based on atmospheric xCO₂ historical data. Also shown the mean results at 25°S based on observations (orange circles for fCO₂ and N-C_T) or calculated from fCO₂ and A_T/SSS (blue triangles) as described in Fig. 10 and listed in Table 4. The monthly pCO₂ and pH (at 25°S–40°E) for 1985–2019 from the CMEMS-LSCE-NN model (Chau et al., 2020) is shown in purple line in (a) and (b). In all figures the orange curves are the reconstructed values assuming ocean fCO₂ in equilibrium with the atmosphere. b: Same as Fig. 11a for the period 1800–2019. For clarity results from the CMEMS-LSCE-NN model for 1985–2019 not shown here.

differences are observed between these cruises conducted 15 years apart and at different seasons. The region was a large CO₂ source in January due to high temperature (30 °C) and near equilibrium in April. In 2019 this region was hit by the strong cyclone “Idai” leading to low salinity and low C_T and A_T concentrations. However, when normalized to salinity, N-C_T concentrations were higher in 2019 compared to 2004 by about 12 (±7) µmol.kg⁻¹, which reflects in part the uptake of anthropogenic CO₂ over 15 years. Surprisingly the fCO₂ (and pH) data at in-situ SST were almost identical in 2004 and 2019, although atmospheric xCO₂ observed onboard increased by +34 ppm. However, when the thermal effect is taken into account, we estimate a small increase in fCO₂ (+11.5 ± 9.8 µatm) and decrease in pH (−0.012 ± 0.008) driven by N-C_T changes. N-A_T concentrations are the same in 2004 and 2019 and do not impact fCO₂ and pH variations. The relatively small difference of fCO₂ between the two cruises is due to seasonal variability that has to be taken into account to detect long-term trends. The decrease in C_T and fCO₂ from January to April is in part due to biological processes. Diazotrophy provides a likely explanation as *Trichodesmium* spp has been observed in abundance in the Mozambique Channel (Dupuy et al., 2016). When the seasonality is taken into account, our observations in 2004 and 2019 reveal an increase in fCO₂ of +1.75 (±0.81) µatm.yr⁻¹, in C_T of +1.04 (±0.79) µmol.kg⁻¹.yr⁻¹ and a decrease of pH of −0.0016.

yr⁻¹ (±0.0015).

The data from these two cruises lead to a robust A_T/SSS relationship in this region that can be used to calculate pH from fCO₂ data from other cruises. We attempted a comparison of our recent observations with sea surface data collected in 1963 in the Mozambique Channel (Keeling and Waterman, 1968). As expected, the fCO₂ was much higher in 2004/2019 than in 1963 (by about 100 µatm) reflecting an atmospheric CO₂ increase by +90 ppm between 1963 and 2019. In addition to anthropogenic CO₂ uptake, long-term ocean warming in this region (+0.11 °C. decade⁻¹) contributes to fCO₂ increase from 1963 to 2019 (by approximately about +10 µatm). For pH, we observed a large decrease in all sectors of the Mozambique Channel, including near coral reef areas in the Eparses Islands (Europa, Juan de Nova). We estimated a mean decrease of −0.104 (±0.006) pH unit between 1963 and 2019, typical of the preindustrial versus modern change in the global ocean (Jiang et al., 2019).

Results from the three cruises (1963, 2004 and 2019) covering a large region (14°S–25°S) are corroborated by three additional observations collected in the southern part of the Mozambique Channel (25°S). Based on those 6 cruises from 1963 to 2019, we evaluated a long-term trend for fCO₂ of +1.55 (±0.11) µatm.yr⁻¹ almost identical to the atmospheric trend. For pH the trend over 1963–2019 is −0.00167.yr⁻¹

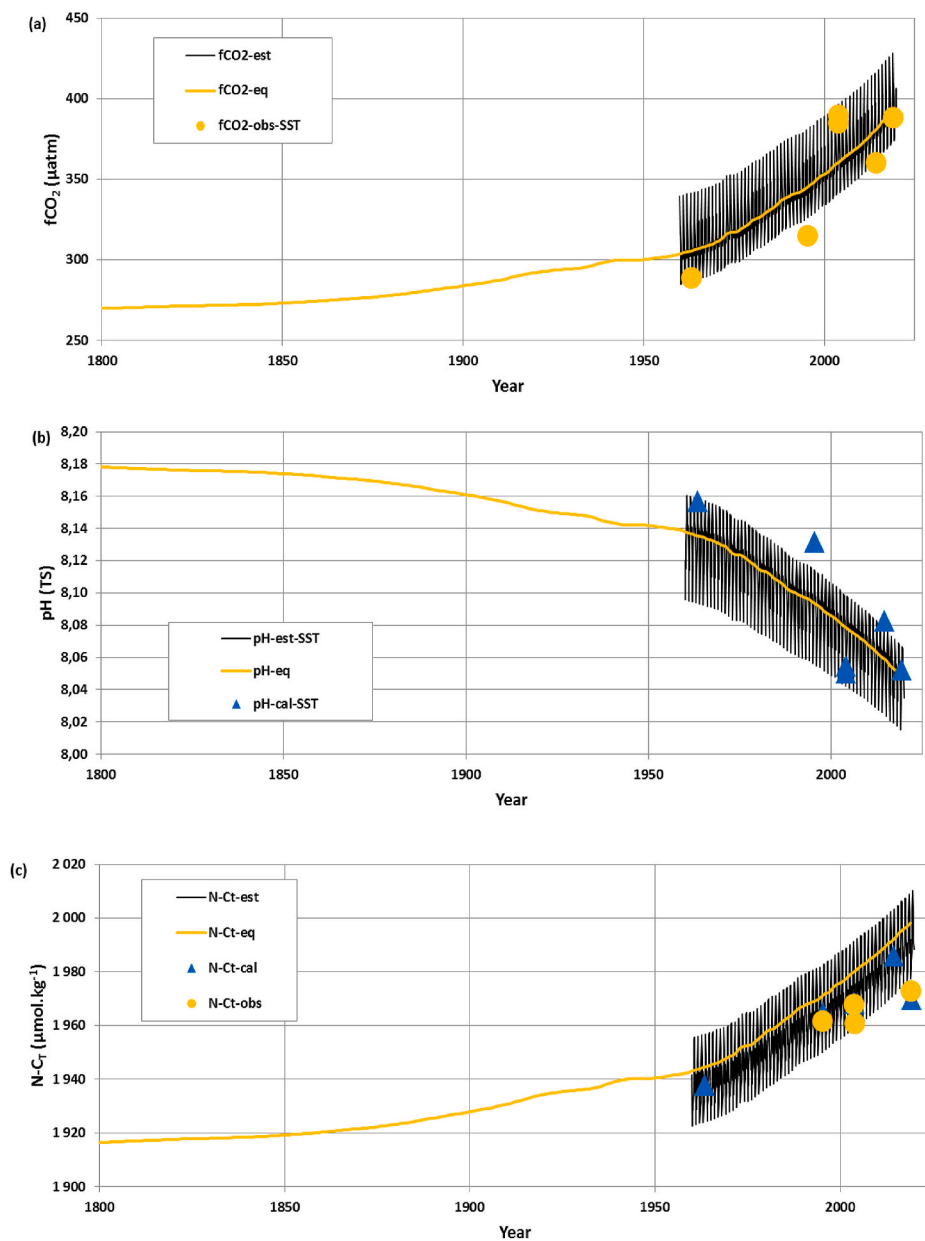


Fig. 13. (continued).

(± 0.0002), and for C_T we estimated an increase of $+1.04 (\pm 0.21) \mu\text{mol.kg}^{-1}.\text{yr}^{-1}$. This is close to the trend of anthropogenic CO_2 evaluated in the upper ocean layers ranging between $+0.93 (\pm 0.13)$ and $+1.00 (\pm 0.04) \mu\text{mol.kg}^{-1}.\text{yr}^{-1}$ depending on the method and data used (Murata et al., 2010; Gruber et al., 2019a, this study). It is worth noting that the $f\text{CO}_2$, pH and C_T trends appear to be more pronounced in the recent decades although this is derived from few cruises only (Table 5). For pH we estimated a trend of $-0.0129.\text{decade}^{-1} (\pm 0.0042)$ over 1963–1995 and $-0.0227.\text{decade}^{-1} (\pm 0.0048)$ for 1995–2019 suggesting an acceleration of acidification. Our different estimates based either on $f\text{CO}_2$ or A_T/C_T measurements in the Mozambique Channel agree with trends in this region derived from global scale reconstructions of $p\text{CO}_2$ and pH (Denvil-Sommer et al., 2019; Chau et al., 2020). We also note that the pH trend in the Mozambique Channel appears lower than previous estimates at basin scale in the Indian Ocean which range between $-0.024.\text{decade}^{-1}$ for the period 1981–2011 and $-0.027.\text{decade}^{-1}$ for 1991–2011 (Lauvset et al., 2015).

The results presented in this analysis aimed at evaluating the change of the carbonate system in the Mozambique Channel at regional scale

and we conclude that the anthropogenic CO_2 emissions are responsible for a significant acidification in surface waters supported here by various sea surface observations and independent anthropogenic CO_2 concentration estimates in the water column. Given the results based on observations since the sixties, we reconstructed the pH change back to the pre-industrial period. In the year 1800, we estimated that pH in the Mozambique Channel was about $8.18 (\pm 0.014)$, i.e. 0.13 higher than in 2019. Concentration of C_T in the year 1800 was likely around $1915 (\pm 10) \mu\text{mol.kg}^{-1}$. These values could serve as a reference for reconstructing pH from coral core samples collected during the CLIM-EPARSES cruise in April 2019 (Tribollet, 2019, 2020).

Our analysis reflects only the change in the open ocean and the “remote” anthropogenic impact through CO_2 emissions. To further evaluate impacts of global environmental change and ocean acidification on coral reefs, a continuous *in situ* sampling program will be needed at higher temporal and spatial scale. It should include the sea level changes either due to global warming or linked to marine heat waves or climate fluctuations such as the Indian Ocean Dipole (IOD) and ENSO in the Pacific (Ampou et al., 2017), the frequency of cyclone events or local

anthropization (especially in Mayotte). In the present analysis, pH was calculated from carbonate system properties, i.e. not from direct pH measurements. In the future and similarly to what is done in other coral reefs areas (Tilbrook et al., 2019), pH should be monitored at high frequency. Detailed analysis of the observations obtained during CLIM-EPARSEs cruise near the Islands and in coral reefs (Juan de Nova, Europa, Mayotte and Glorieuses) will be investigated in further studies.

Author's contribution

Claire Lo Monaco: Co-PI of the on-going OISO project, measured and qualified the fCO_2 , A_T and C_T data for OISO-11 and CLIM-EPARSEs cruises, contributed to the interpretation of the results and the writing of the manuscript. Nicolas Metzl is Co-PI of the on-going OISO project, was Chief scientist of the OISO-11 cruise, measured and qualified the fCO_2 , A_T and C_T data for OISO-11 cruise, qualified the fCO_2 , A_T and C_T data for CLIM-EPARSEs cruise, interpreted the results, wrote the draft of the manuscript and prepared the figures. Jonathan Fin measured the fCO_2 , A_T and C_T properties and helped for sampling during CLIM-EPARSEs cruise. Claude Mignon: measured the fCO_2 , A_T and C_T properties and helped for sampling during CLIM-EPARSEs cruise. Pascale Cuet: measured and qualified the Chl-a samples for CLIM-EPARSEs cruise, contributed to the interpretation of the results and the writing of the manuscript. Eric Douville: helped for the sampling during CLIM-EPARSEs cruise and contributed to the writing of the manuscript. Marion Gehlen: provided the neural network model results, contributed to the statistics, to the interpretation of the results and the writing of the manuscript. Trang Chau: provided the neural network model results, contributed to the statistics and prepared some figures and tables in the Supplementary material. Aline Tribollet: is PI of the ongoing CLIM-EPARSEs project, was Chief scientist of the CLIM-EPARSEs cruise and contributed to the interpretation of the results and the writing of the manuscript.

Declaration of competing interest

The authors declare that they have no known competing financial interests or personal relationships that could have appeared to influence the work reported in this paper.

Acknowledgments

The OISO program was supported by the French institutes INSU (Institut National des Sciences de l'Univers) and IPEV (Institut Polaire Paul-Emile Victor), the French program SOERE/Great-Gases, and the European programs CARBOOCEAN (grant 511176) and CARBOCHANGE (grant 264879). The CLIM-EPARSEs project is supported by TAAF (Terres Australes et Antarctiques Françaises), IRD (Institut de Recherche pour le Développement), Fondation Prince Albert II de Monaco (www.fpa2.org), INSU (Institut National des Sciences de l'Univers), CNRS (Centre National de Recherche Scientifique), Museum National d'Histoire Naturelle (MNHN), UMRs LOCEAN-IPSL, ENTROPIE and LSCE. We thank the captains and crew of R.R.V. *Marion Dufresne* and the staff at the French Polar Institute (IPEV). The development of the neural network model benefited from funding by the French INSU-GMMC project "PPR-Green-Grog (grant no 5-DS-PPR-GGREGO), the EU H2020 project AtlantOS (grant no 633211), as well as through the Copernicus Marine Environment Monitoring Service (project CMEMS-TAC-MOB). Anna Conchon contributed to the development and computation of pCO_2 and pH reconstructions. The Surface Ocean CO₂ Atlas (SOCAT, www.socat.info) is an international effort, endorsed by the International Ocean Carbon Coordination Project (IOCCP), the Surface Ocean Lower Atmosphere Study (SOLAS) and the Integrated Marine Biogeochemistry and Ecosystem Research program (IMBER), to deliver a uniformly quality-controlled surface ocean CO₂ database. We thank the two anonymous reviewers for making constructive

suggestions, which resulted in improvements of this paper and Raleigh Hood, Editor of this IIOE-2 special issue.

Appendix A. Supplementary data

Supplementary data to this article can be found online at <https://doi.org/10.1016/j.dsr2.2021.104936>.

References

- Alory, G., Wijffels, S., Meyers, G., 2007. Observed temperature trends in the Indian Ocean over 1960–1999 and associated mechanisms. *Geophys. Res. Lett.* 34, L20606. <https://doi.org/10.1029/2006GL028044>.
- Álvarez, M., Lo Monaco, C., Tanhua, T., Yool, A., Oschlies, A., Bullister, J.L., Goyet, C., Metzl, N., Touratier, F., McDonagh, E., Bryden, H.L., 2009. Estimating the storage of anthropogenic carbon in the subtropical Indian Ocean: a comparison of five different approaches. *Biogeosciences* 6, 681–703. <https://doi.org/10.5194/bg-6-681-2009>.
- Aminot, A., Kérouel, R., 2004. *Hydrologie des écosystèmes marins: paramètres et analyses*. Ifremer, p. 336.
- Ampou, E.E., Johan, O., Menkes, C.E., Niño, F., Birol, F., Ouillon, S., Andréfouët, S., 2017. Coral mortality induced by the 2015–2016 El-Niño in Indonesia: the effect of rapid sea level fall. *Biogeosciences* 14, 817–826. <https://doi.org/10.5194/bg-14-817-2017>.
- Antonov, J.I., Locarnini, R.A., Boyer, T.P., Mishonov, A.V., Garcia, H.E., 2006. *World Ocean Atlas 2005*. In: Levitus, S. (Ed.), Volume 2: Salinity. NOAA Atlas NESDIS 62, US Government Printing Office, Washington, DC, p. 182.
- Bakker, D.C.E., Pfeil, B., Smith, K., Hankin, S., Olsen, A., Alin, S.R., Cosca, C., Harasawa, S., Kozyr, A., Nojiri, Y., O'Brien, K.M., Schuster, U., Telszewski, M., Tilbrook, B., Wada, C., Akl, J., Barbero, L., Bates, N.R., Boutin, J., Bozec, Y., Cai, W.-J., Castle, R.D., Chavez, F.P., Chen, L., Chierici, M., Currie, K., de Baar, H.J.W., Evans, W., Feely, R.A., Fransson, A., Gao, Z., Hales, B., Hardman-Mountford, N.J., Hoppema, M., Huang, W.-J., Hunt, C.W., Huss, B., Ichikawa, T., Johannessen, T., Jones, E.M., Jones, S.D., Jutterström, S., Kitidis, V., Körtzinger, A., Landschützer, P., Lauvset, S.K., Lefèvre, N., Manke, A.B., Mathis, J.T., Merlivat, L., Metzl, N., Murata, A., Newberger, T., Omar, A.M., Ono, T., Park, G.-H., Paterson, K., Pierrot, D., Ríos, A.F., Sabine, C.L., Saito, S., Salisbury, J., Sarma, V.V.S.S., Schlitzer, R., Sieger, R., Skjelvan, I., Steinhoff, T., Sullivan, K.F., Sun, H., Sutton, A. J., Suzuki, T., Sweeney, C., Takahashi, T., Tjiputra, J., Tsurushima, M., van Heuven, S.M.A.C., Vandemark, D., Vlahos, P., Wallace, D.W.R., Wanninkhof, R., Watson, A.J., 2014. An update to the surface ocean CO₂ Atlas (SOCAT version 2). *Earth Syst. Sci. Data* 6, 69–90. <https://doi.org/10.5194/essd-6-69-2014>.
- Bakker, D.C.E., Pfeil, B., Landa, C.S., Metzl, N., O'Brien, K.M., Olsen, A., Smith, K., Cosca, C., Harasawa, S., Jones, S.D., Nakaoka, S.-I., Nojiri, Y., Schuster, U., Steinhoff, T., Sweeney, C., Takahashi, T., Tilbrook, B., Wada, C., Wanninkhof, R., Alin, S.R., Balestrini, C.F., Barbero, L., Bates, N.R., Bianchi, A.A., Bonou, F., Boutin, J., Bozec, Y., Burger, E.F., Cai, W.-J., Castle, R.D., Chen, L., Chierici, M., Currie, K., Evans, W., Featherstone, C., Feely, R.A., Fransson, A., Goyet, C., Greenwood, N., Gregor, L., Hankin, S., Hardman-Mountford, N.J., Harlay, J., Hauck, J., Hoppema, M., Humphreys, M.P., Hunt, C.W., Huss, B., Ibánhez, J.S.P., Johannessen, T., Keeling, R., Kitidis, V., Körtzinger, A., Kozyr, A., Krasakopoulou, E., Kuwata, A., Landschützer, P., Lauvset, S.K., Lefèvre, N., Lo Monaco, C., Manke, A., Mathis, J.T., Merlivat, L., Millero, F.J., Monteiro, P.M.S., Munro, D.R., Murata, A., Newberger, T., Omar, A.M., Ono, T., Paterson, K., Pearce, D., Pierrot, D., Robbins, L. L., Saito, S., Salisbury, J., Schlitzer, R., Schneider, R., Schweitzer, R., Sieger, R., Skjelvan, I., Sullivan, K.F., Sutherland, S.C., Sutton, A.J., Tadokoro, K., Telszewski, M., Tuma, M., Van Heuven, S.M.A.C., Vandemark, D., Ward, B., Watson, A.J., Xu, S., 2016. A multi-decade record of high-quality fCO_2 data in version 3 of the Surface Ocean CO₂ Atlas (SOCAT). *Earth Syst. Sci. Data* 8, 383–413. <https://doi.org/10.5194/essd-8-383-2016>.
- Bakker, D.C.E., et al., 2020. Surface Ocean CO₂ Atlas Database Version 2020 (SOCATv2020) (NCEI Accession 0210711). NOAA National Centers for Environmental Information. Dataset. <https://doi.org/10.25921/4xkx-ss49>. Last Access 15/6/2020.
- Bates, N.R., Pequignat, A.C., Sabine, C.L., 2006. Ocean carbon cycling in the Indian Ocean: 1. Spatiotemporal variability of inorganic carbon and air-sea CO₂ gas exchange. *Global Biogeochem. Cycles* 20, GB3020. <https://doi.org/10.1029/2005GB002491>.
- Bates, N., Astor, Y., Church, M., Currie, K., Dore, J., Gonaález-Dávila, M., Lorenzoni, L., Muller-Karger, F., Olafsson, J., Santa-Casiano, M., 2014. A time-series view of changing ocean chemistry due to ocean uptake of anthropogenic CO₂ and ocean acidification. *Oceanography* 27 (1), 126–141. <https://doi.org/10.5670/oceanog.2014.16>.
- Beaufort, L., Probert, I., de Garidel-Thoron, T., Bendif, E.M., Ruiz-Pino, D., Metzl, N., Goyet, C., Buchet, N., Coupel, P., Grelaud, M., Rost, B., Rickaby, R.E.M., de Vargas, C., 2011. Sensitivity of coccolithophores to carbonate chemistry and ocean acidification. *Nature*. <https://doi.org/10.1038/nature10295>.
- Boyd, P.W., Collins, S., Dupont, S., Fabricius, K., Gattuso, J.-P., Havenhand, J., Hutchins, D.A., Riebesell, U., Rintoul, M.S., Vichi, M., Biswas, H., Ciotti, A., Gao, K., Gehlen, M., Hurd, C.L., Kurihara, H., McGraw, C.M., Navarro, J.M., Nilsson, G.E., Passow, U., Pörtner, H.-O., 2018. Experimental strategies to assess the biological ramifications of multiple drivers of global ocean change—a review. *Glob Change Biol.* 24, 2239–2261. <https://doi.org/10.1111/gcb.14102>.

- Carter, B.R., Williams, N.L., Gray, A.R., Feely, R.A., 2016. Locally interpolated alkalinity regression for global alkalinity estimation. *Limnol Oceanogr. Methods* 14, 268–277. <https://doi.org/10.1002/lom3.10087>.
- Carter, B.R., Feely, R.A., Williams, N.L., Dickson, A.G., Fong, M.B., Takeshita, Y., 2018. Updated methods for global locally interpolated estimation of alkalinity, pH, and nitrate. *Limnol Oceanogr. Methods* 16, 119–131. <https://doi.org/10.1002/lom3.10232>.
- Chau, T.T., Gehlen, M., Chevallier, F., 2020. Global Ocean Surface Carbon Product MULTIOBS_GLO_BIO_CARBON_SURFACE_REP_015_008. E.U. Copernicus Marine Service Information. https://resources.marine.copernicus.eu/documents/QUID/CM_EMS-MOB-QUID-015-008.pdf.
- Chauvin, A., Denis, V., Cuet, P., 2011. Is the response of coral calcification to seawater acidification related to nutrient loading? *Coral Reefs* 30, 911. <https://doi.org/10.1007/s00338-011-0786-7>.
- Copin-Montégut, C., 1988. A new formula for the effect of temperature on the partial pressure of CO₂ in seawater. *Mar. Chem.* 25, 29–37. [https://doi.org/10.1016/0304-4203\(88\)90012-6](https://doi.org/10.1016/0304-4203(88)90012-6).
- Copin-Montégut, C., 1989. A new formula for the effect of temperature on the partial pressure of CO₂ in seawater. *Corrigendum. Marine Chem.* 27, 143–144. [https://doi.org/10.1016/0304-4203\(89\)90034-0](https://doi.org/10.1016/0304-4203(89)90034-0).
- Cuny-Guirric, K., Douville, E., Reynaud, S., Allemand, D., Bordier, L., Canesi, M., Mazzoli, C., Taviani, M., Canese, F., McCulloch, M., Trotter, J., Rico-Esenaño, S.D., Sanchez-Cabeza, J.A., Ruiz-Fernández, A.C., Carricart-Ganivet, J.P., Scott, P., Sadekov, A., Montagna, P., 2019. Coral Li/Mg thermometry: caveats and constraints. *Chem. Geol.* 523, 162–178. <https://doi.org/10.1016/j.chemgeo.2019.03.038>.
- Cyronak, T., Schulz, K.G., Santos, I.R., Eyre, B.D., 2014. Enhanced acidification of global coral reefs driven by regional biogeochemical feedbacks. *Geophys. Res. Lett.* <https://doi.org/10.1002/2014GL060849>, 2014GL060849.
- Cyronak, T., Takeshita, Y., Courtney, T.A., DeCarlo, E.H., Eyre, B.D., Kline, D.I., Martz, T., Page, H., Price, N.N., Smith, J., Stoltenberg, L., Tresguerres, M., Andersson, A.J., 2020. Diel temperature and pH variability scale with depth across diverse coral reef habitats. *Limnol. Oceanogr.* 5, 193–203. <https://doi.org/10.1002/lol2.10129>.
- D'Olivio, J.P., Ellwood, G., DeCarlo, T.M., McCulloch, M.T., 2019. Deconvolving the long-term impacts of ocean acidification and warming on coral biomineralisation. *Earth Planet Sci. Lett.* 526, 115785. <https://doi.org/10.1016/j.epsl.2019.115785>.
- de Moel, H., Ganssen, G.M., Peeters, F.J.C., Jung, S.J.A., Kroon, D., Brummer, G.J.A., Zeebe, R.E., 2009. Planktic foraminiferal shell thinning in the Arabian Sea due to anthropogenic ocean acidification? *Biogeosciences* 6, 1917–1925. <https://doi.org/10.5194/bg-6-1917-2009>.
- Denvil-Sommer, A., Gehlen, M., Vrac, M., Mejia, C., 2019. LSCE-FFNN-v1: a two-step neural network model for the reconstruction of surface ocean pCO₂ over the global ocean. *Geosci. Model Dev. (GMD)* 12, 2091–2105. <https://doi.org/10.5194/gmd-12-2091-2019>.
- Dickson, A.G., 1990. Standard potential of the reaction: AgCl(s) + ½H₂(g) = Ag(s) + HCl(aq), and the standard acidity constant of the ion HSO₄⁻ in synthetic sea water from 273.15 to 318.15 K. *J. Chem. Thermodyn.* 22, 113–127. [https://doi.org/10.1016/0021-9614\(90\)90074-z](https://doi.org/10.1016/0021-9614(90)90074-z).
- Dickson, A.G., Millero, F.J., 1987. A comparison of the equilibrium constants for the dissociation of carbonic acid in seawater media. *Deep Sea Res.* 34 (10), 1733–1743. [https://doi.org/10.1016/0198-0149\(87\)90021-5](https://doi.org/10.1016/0198-0149(87)90021-5).
- Dickson, A.G., Sabine, C.L., Christian, J.R. (Eds.), 2007. *Guide to Best Practices for Ocean CO₂ Measurements*, 3. PICES Special Publication, p. 191.
- Dlugokencky, E., Tans, P., 2020. Trends in Atmospheric Carbon Dioxide. National Oceanic & Atmospheric Administration, Earth System Research Laboratory (NOAA/ESRL) available at: <http://www.esrl.noaa.gov/gmd/ccgg/trends/global.html>. (Accessed 22 February 2020). last access:
- Doney, S.C., Fabry, V.J., Feely, R.A., Kleypas, J.A., 2009. Ocean acidification: the other CO₂ problem. *Annual. Rev. Marine Sci.* 1 (1), 169–192. <https://doi.org/10.1146/annurev.marine.010908.163834>.
- Dupuy, C., Pagano, M., Got, P., Domaizon, I., Chappuis, A., Marchessaux, G., Bouvy, M., 2016. Trophic relationships between metazooplankton communities and their plankton food sources in the Iles Eparses (Western Indian Ocean). *Mar. Environ. Res.* 116, 18–31. <https://doi.org/10.1016/j.marenvres.2016.02.011>.
- Edmond, J.M., 1970. High precision determination of titration alkalinity and total carbon dioxide content of sea water by potentiometric titration. *Deep-Sea Res.* 17, 737–750. [https://doi.org/10.1016/0011-7471\(70\)90038-0](https://doi.org/10.1016/0011-7471(70)90038-0).
- Eyre, B.D., Cyronak, T., Drupp, P., De Carlo, E.H., Sachs, J.P., Andersson, A.J., 2018. Coral reefs will transition to net dissolving before end of century. *Science* 359 (6378), 908–911. <https://doi.org/10.1126/science.aao1118>.
- Fabry, V.J., Seibel, B.A., Feely, R.A., Orr, J.C., 2008. Impacts of ocean acidification on marine fauna and ecosystem processes. *ICES J. Mar. Sci.* 65, 414–432. <https://doi.org/10.1093/icesjms/fsn048>.
- Feely, R.A., Doney, S.C., Cooley, S.R., 2009. Ocean acidification: present conditions and future changes in a high-CO₂ world. *Oceanography* 22 (4), 36–47. <https://doi.org/10.5670/oceanog.2009.95>.
- Friedlingstein, P., Jones, M.W., O'Sullivan, M., Andrew, R.M., Hauck, J., Peters, G.P., Peters, W., Pongratz, J., Sitoh, S., Le Quééré, C., Bakker, D.C.E., Canadell, J.G., Ciais, P., Jackson, R.B., Anthoni, P., Barbero, L., Bastos, A., Bastrikov, V., Becker, M., Bopp, L., Buitenhuis, E., Chandra, N., Chevallier, F., Chini, L.P., Currie, K.I., Feely, R.A., Gehlen, M., Gilfillan, D., Gkritzalis, T., Goll, D.S., Gruber, N., Gutekunst, S., Harris, I., Havard, V., Houghton, R.A., Hurtt, G., Ilyina, T., Jain, A.K., Joetzer, E., Kaplan, J.O., Kato, E., Klein Goldewijk, K., Korsbakken, J.I., Landschützer, P., Lauvset, S.K., Lefevre, N., Lenton, A., Liernert, S., Lombardozzi, D., Marland, G., McGuire, P.C., Melton, J.R., Metz, N., Munro, D.R., Nabel, J.E.M.S., Nakaoka, S.-I., Neill, C., Omar, A.M., Ono, T., Peregon, A., Pierrot, D., Poulter, B., Rehder, G., Resplandy, L., Robertson, E., Rödenbeck, C., Séférian, R., Schwinger, J., Smith, N., Tans, P.P., Tian, H., Tilbrook, B., Tubiello, F.N., van der Werf, G.R., Wiltshire, A.J., Zaehele, S., 2019. Global carbon budget 2019. *Earth Syst. Sci. Data* 11, 1783–1838. <https://doi.org/10.5194/essd-11-1783-2019>.
- Garcia, H.E., Locarnini, R.A., Boyer, T.P., Antonov, J.I., Baranova, O.K., Zweng, M.M., Reagan, J.R., Johnson, D.R., 2014. *World Ocean Atlas 2013, Volume 4: dissolved inorganic nutrients (phosphate, nitrate, silicate)*. In: Levitus, S., Mishonov Technical, A. (Eds.), *NOAA Atlas NESDIS*, 76, p. 25.
- Gattuso, J.-P., Magnan, A., Billé, R., Cheung, W.W.L., Howes, E.L., Joos, F., Allemand, D., Bopp, L., Cooley, S., Eakin, M., Hoegh-Guldberg, O., Kelly, R.P., Pörtner, H.-O., Rogers, A.D., Baxter, J.M., Laffoley, D., Osborn, D., Rankovic, A., Rochette, J., Sumaila, U.R., Treyer, S., Turley, C., 2015. Contrasting futures for ocean and society from different anthropogenic CO₂ emissions scenarios. *Science* 349, aac4722. <https://doi.org/10.1126/science.aac4722>.
- Gruber, N., Clement, D., Carter, B.R., Feely, R.A., van Heuven, S., Hoppema, M., Ishii, M., Key, R.M., Kozyr, A., Lauvset, S.K., Lo Monaco, C., Mathis, J.T., Murata, A., Olsen, A., Perez, F.F., Sabine, C.L., Tanhua, T., Wanninkhof, R., 2019a. The oceanic sink for anthropogenic CO₂ from 1994 to 2007. *Science* 363 (6432), 1193–1199. <https://doi.org/10.1126/science.aau5153>.
- Gruber, N., Clement, D., Carter, B.R., Feely, R.A., Heuven, S. van, Hoppema, M., Ishii, M., Key, R.M., Kozyr, A., Lauvset, S.K., Lo Monaco, C., Mathis, J.T., Murata, A., Olsen, A., Perez, F.F., Sabine, C.L., Tanhua, T., Wanninkhof, R., 2019b. The Oceanic Sink for Anthropogenic CO₂ from 1994 to 2007 - the Data (NCEI Accession 0186034). NOAA National Centers for Environmental Information. Dataset. <https://doi.org/10.25921/wdn2-pt10>. (Accessed 17 February 2020). last access:
- Halo, I., Backeberg, B., Penven, P., Ansong, I., Reason, C., Ullgren, J.E., 2014. Eddy properties in the Mozambique Channel: a comparison between observations and two numerical ocean circulation models. *Deep Sea Res. Part II Top. Stud. Oceanogr.* 100, 38–53. <https://doi.org/10.1016/j.dsr2.2013.10.015>.
- Hancke, L., Roberts, M.J., TERNON, J.F., 2014. Surface drifter trajectories highlight flow pathways in the Mozambique Channel. *Deep Sea Res. Part II Top. Stud. Oceanogr.* 100, 27–37. <https://doi.org/10.1016/j.dsr2.2013.10.014>.
- Hansson, I., 1973. The determination of dissociation constants of carbonic acid in synthetic sea water in the salinity range of 20–40‰ and temperature range of 5–30°C. *Acta Chem. Scand.* 27, 931–944. <https://doi.org/10.3891/acta.chem.scand.27-0931>.
- Hoegh-Guldberg, O., Mumby, P.J., Hooten, A.J., Steneck, R.S., Greenfield, P., Gomez, E., Harvell, C.D., Sale, P.F., Edwards, A.J., Caldeira, K., Knowlton, N., Eakin, C.M., Iglesias-Prieto, R., Muthiga, N., Bradbury, R.H., Dubi, A., Hatziolos, M.E., 2007. Coral reefs under rapid climate change and ocean acidification. *Science* 14, 1737–1742. <https://doi.org/10.1126/science.1152509>.
- Hofmann, G.E., Smith, J.E., Johnson, K.S., Send, U., Levin, L.A., et al., 2011. High-frequency dynamics of ocean pH: a multi-ecosystem comparison. *PLoS One* 6 (12), e28983. <https://doi.org/10.1371/journal.pone.0028983>.
- Iida, Y., Takatani, Y., Kojima, A., Ishii, M., 2020. Global trends of ocean CO₂ sink and ocean acidification: an observation-based reconstruction of surface ocean inorganic carbon variables. *J. Oceanogr.* <https://doi.org/10.1007/s10872-020-00571-5>.
- IPCC, 2019. In: Pörtner, H.-O., Roberts, D.C., Masson-Delmotte, V., Zhai, P., Tignor, M., Poloczanska, E., Mintenbeck, K., Nicolai, M., Okem, A., Petzold, J., Rama, B., Weyer, N. (Eds.), *IPCC Special Report on the Ocean and Cryosphere in a Changing Climate* (in press).
- Ishii, M., Kosugi, N., Sasano, D., Saito, S., Midorikawa, T., Inoue, H.Y., 2011. Ocean acidification off the south coast of Japan: a result from time series observations of CO₂ parameters from 1994 to 2008. *J. Geophys. Res.* 116, C06022. <https://doi.org/10.1029/2010JC006831>.
- Jabaud-Jan, A., Metzl, N., Brunet, C., Poisson, A., Schauer, B., 2004. Interannual variability of the carbon dioxide system in the southern Indian Ocean (20°S–60°S): the impact of a warm anomaly in austral summer 1998. *Global Biogeochem. Cycles* 18 (1). <https://doi.org/10.1029/2002GB002017>.
- Jiang, L.-Q., Carter, B.R., Feely, R.A., Lauvset, S.K., Olsen, A., 2019. Surface ocean pH and buffer capacity: past, present and future. *Sci. Rep.* 9 (1), 1–11. <https://doi.org/10.1038/s41598-019-55039-4>.
- Kapsenberg, L., Allouane, S., Gazeau, F., Mousseau, L., Gattuso, J.-P., 2017. Coastal ocean acidification and increasing total alkalinity in the northwestern Mediterranean Sea. *Ocean Sci.* 13, 411–426. <https://doi.org/10.5194/os-13-411-2017>.
- Keeling, C.D., Waterman, L.S., 1968. Carbon dioxide in surface ocean waters: 3. Measurements on Lusiad Expedition 1962–1963. *J. Geophys. Res.* 73 (14), 4529–4541. <https://doi.org/10.1029/JB073i014p04529>.
- Key, R., Olsen, A., Van Heuven, S., Lauvset, S., Velo, A., Lin, X., Schirnick, C., Kozyr, A., Tanhua, T., Hoppema, M., Jutterstrom, S., Steinfeldt, R., Jeansson, E., Ishii, M., Perez, F., Suzuki, T., 2015. Global Ocean Data Analysis Project, Version 2 (GLODAPv2), ORNL/CDIAC-162, ND-P093, Dataset. <https://doi.org/10.3334/CDIAC/OTG.NDPO93.GLODAPv2>.
- Kleypas, J.A., Buddemeier, R.W., Archer, D., Gattuso, J.-P., Langdon, C., Opdyke, B.N., 1999. Geochemical consequences of increased atmospheric carbon dioxide on coral reefs. *Science* 284 (5411), 118–120. <https://doi.org/10.1126/science.284.5411.118>.
- Kwiatkowski, L., Orr, J.C., 2018. Diverging seasonal extremes for ocean acidification during the twenty-first century. *Nat. Clim. Change.* <https://doi.org/10.1038/s41558-017-0054-0>.
- Lauvset, S.K., Gruber, N., Landschützer, P., Olsen, A., Tjiputra, J., 2015. Trends and drivers in global surface ocean pH over the past 3 decades. *Biogeosciences* 12, 1285–1298. <https://doi.org/10.5194/bg-12-1285-2015>.
- Lauvset, S., Currie, K., Metzl, N., Nakaoka, S., Bakker, D., Sullivan, K., Sutton, A., O'Brien, K., Olsen, A., 2019. SOCAT Quality Control Cookbook for SOCAT Version 7. Int. Report. Available at www.socat.info.

- Lee, K., Tong, L.T., Millero, F.J., Sabine, C.L., Dickson, A.G., Goyet, C., Park, G.H., Wanninkhof, R., Feely, R.A., Key, R.M., 2006. Global relationships of total alkalinity with salinity and temperature in surface waters of the world's oceans. *Geophys. Res. Lett.* 33, L19605. <https://doi.org/10.1029/2006GL027207>.
- Lewis, E., Wallace, D.W.R., 1998. Program Developed for CO₂ System Calculations. ORNL/CDIAC-105. Carbon Dioxide Information Analysis Center. Oak Ridge National Laboratory, US. Dept. of Energy, Oak Ridge, TN.
- Liu, Y., Peng, Z., Zhou, R., Song, S., Liu, W., You, C.-F., Lin, Y.-P., Yu, K., Wu, C.-C., Wei, G., Xie, L., Burr, G.S., Shen, C.-C., 2014. Acceleration of modern acidification in the South China Sea driven by anthropogenic CO₂. *Sci. Rep.* 4, 5148. <https://doi.org/10.1038/srep05148>.
- Lo Monaco, C., Álvarez, M., Key, R.M., Lin, X., Tanhua, T., Tilbrook, B., Bakker, D.C.E., van Heuven, S., Hoppema, M., Metz, N., Ríos, A.F., Sabine, C.L., Velo, A., 2010. Assessing the internal consistency of the CARINA database in the Indian sector of the Southern Ocean. *Earth Syst. Sci. Data* 2, 51–70. <https://doi.org/10.5194/essd-2-51-2010>.
- Lo Monaco, C., Metz, N., Tribollet, A., 2020a. Sea Surface Measurements of Fugacity of CO₂ (fCO₂), Temperature and Salinity during the Cruise CLIM-EPARSES (EXPOCODE 35MV20190405) Onboard R/V Marion-Dufresne in the Indian Ocean and Mozambique Channel from 2019-04-04 to 2019-04-30 (NCEI Accession 0208809). NOAA National Centers for Environmental Information. Dataset. <https://accession.nodc.noaa.gov/0208809>.
- Lo Monaco, C., Metz, N., Fin, J., Tribollet, A., 2020b. Sea Surface Measurements of Dissolved Inorganic Carbon (DIC) and Total Alkalinity (TALK), Temperature and Salinity during the R/V Marion-Dufresne Cruise CLIM-EPARSES (EXPOCODE 35MV20190405) in the Indian Ocean and Mozambique Channel from 2019-04-04 to 2019-04-30. (NCEI Accession 0212218). [indicate Subset Used]. NOAA National Centers for Environmental Information. Dataset. <https://accession.nodc.noaa.gov/0212218>.
- Louanchi, F., Metz, N., Poisson, A., 1996. Modelling the monthly sea surface fCO₂ fields in the Indian Ocean. *Mar. Chem.* 55, 265–279. [https://doi.org/10.1016/S0304-4203\(96\)00066-7](https://doi.org/10.1016/S0304-4203(96)00066-7).
- Lueker, T.J., Dickson, A.G., Keeling, C.D., 2000. Ocean pCO₂ calculated from dissolved inorganic carbon, alkalinity, and equations for K-1 and K-2: validation based on laboratory measurements of CO₂ in gas and seawater at equilibrium. *Mar. Chem.* 70, 105–119. [https://doi.org/10.1016/S0304-4203\(00\)00022-0](https://doi.org/10.1016/S0304-4203(00)00022-0).
- McKinna, L.I.W., 2015. Three decades of ocean-color remote-sensing *Trichodesmium* spp. in the World's oceans: a review. *Prog. Oceanogr.* 131, 177–199. <https://doi.org/10.1016/j.pcean.2014.12.013>.
- Mehrbach, C., Culbertson, C.H., Hawley, J.E., Pytkowicz, R.M., 1973. Measurement of the apparent dissociation constants of carbonic acid in seawater at atmospheric pressure. *Limnol. Oceanogr.* 18, 897–907. <https://doi.org/10.4319/lo.1973.18.6.0897>.
- Meinshausen, M., Vogel, E., Nauels, A., Lorbacher, K., Meinshausen, N., Etheridge, D.M., Fraser, P.J., Montzka, S.A., Rayner, P.J., Trudinger, C.M., Krummel, P.B., Beyerle, U., Canadell, J.G., Daniel, J.S., Enting, I.G., Law, R.M., Lunder, C.R., O'Doherty, S., Prinn, R.G., Reimann, S., Rubino, M., Velders, G.J.M., Vollmer, M.K., Wang, R.H.J., Weiss, R., 2017. Historical greenhouse gas concentrations for climate modelling (CMIP6). *Geosci. Model Dev. (GMD)* 10, 2057–2116. <https://doi.org/10.5194/gmd-10-2057-2017>.
- Metz, N., 2009. Decadal increase of oceanic carbon dioxide in the Southern Indian Ocean surface waters (1991–2007). *Deep Sea Res. Part II Top. Stud. Oceanogr.* 56 (8–10), 607–619. <https://doi.org/10.1016/j.dsr2.2008.12.007>.
- Metz, N., 2018. Carbon Dioxide, Temperature, Salinity, and Other Variables Collected via Surface Underway Survey from Volunteer Observing Ship Marion Dufresne in the Indian Ocean and Southern Oceans (> 60 Degrees South) from 2004-01-06 to 2004-02-08 (NCEI Accession 0080996). NOAA National Centers for Environmental Information. Dataset. https://doi.org/10.3334/cdiac/otg.vos_oiso_11.
- Metz, N., Lo Monaco, C., 2018. Sea Surface Measurements of Dissolved Inorganic Carbon (DIC), Total Alkalinity (TALK), Temperature and Salinity during the R/V Marion-Dufresne Ocean Indien Service d'Observations - 11 (OISO-11) Cruise (EXPOCODE 35MV20040106) in the Indian Ocean from 2004-01-06 to 2004-02-08 (NCEI Accession 0173515). Version 1.1. NOAA National Centers for Environmental Information. Dataset. <https://doi.org/10.7289/V52805Z3>.
- Metz, N., Poisson, A., Louanchi, F., Brunet, C., Schauer, B., Bres, B., 1995. Spatio-temporal distributions of air-sea fluxes of CO₂ in the Indian and Antarctic oceans. *Tellus B* 47 (1–2), 56–69. <https://doi.org/10.3402/tellusb.v47i1-2.16006>.
- Metz, N., Louanchi, F., Poisson, A., 1998. Seasonal and interannual variations of sea surface carbon dioxide in the subtropical Indian ocean. *Mar. Chem.* 60, 131–146. [https://doi.org/10.1016/S0304-4203\(98\)00083-8](https://doi.org/10.1016/S0304-4203(98)00083-8).
- Metz, N., Brunet, C., Jabaud-Jan, A., Poisson, A., Schauer, B., 2006. Summer and winter air-sea CO₂ fluxes in the Southern Ocean. *Deep Sea Res. I* 53, 1548–1563. <https://doi.org/10.1016/j.dsr.2006.07.006>.
- Millero, F.J., Lee, K., Roche, M., 1998. Distribution of alkalinity in the surface waters of the major oceans. *Mar. Chem.* 60, 111–130. [https://doi.org/10.1016/S0304-4203\(97\)00084-4](https://doi.org/10.1016/S0304-4203(97)00084-4).
- Mollica, N.R., Guo, W., Cohen, A.L., Huang, K.F., Foster, G.L., Donald, H.K., Solow, A.R., 2018. Ocean acidification affects coral growth by reducing skeletal density. *Proc. Natl. Acad. Sci. Unit. States Am.* 115 (8), 1754–1759. <https://doi.org/10.1073/pnas.1712806115>.
- Montagna, P., McCulloch, M., Douville, E., López Correa, M., Trotter, J., Rodolfo-Metalpa, R., Dissard, D., Ferrier-Pagès, C., Frank, N., Freiwald, A., Goldstein, S., Mazzoli, C., Reynaud, S., Rüggeberg, A., Russo, S., Taviani, M., 2014. Li/Mg systematics in scleractinian corals: calibration of the thermometer. *Geochim. Cosmochim. Acta* 132, 288–310. <https://doi.org/10.1016/j.gca.2014.02.005>.
- Moutin, T., Wagener, T., Caffin, M., Fumenia, A., Gimenez, A., Baklouti, M., Bouruet-Aubertot, P., Pujol-Pay, M., Leblanc, K., Lefevre, D., Helias Nunige, S., Leblond, N., Grosso, O., de Verneil, A., 2018. Nutrient availability and the ultimate control of the biological carbon pump in the western tropical South Pacific Ocean. *Biogeosciences* 15, 2961–2989. <https://doi.org/10.5194/bg-15-2961-2018>.
- Murata, A., Kumamoto, Y., Sasaki, K., Watanabe, S., Fukasawa, M., 2010. Decadal increases in anthropogenic CO₂ along 20°S in the south Indian ocean. *J. Geophys. Res.* 115, C12055. <https://doi.org/10.1029/2010JC006250>.
- Olsen, A., Key, R.M., van Heuven, S., Lauvset, S.K., Velo, A., Lin, X., Schirnack, C., Kozyr, A., Tanhua, T., Hoppema, M., Jutterström, S., Steinfeldt, R., Jeansson, E., Ishii, M., Pérez, F.F., Suzuki, T., 2016. An internally consistent data product for the world ocean: the Global Ocean Data Analysis Project, version 2 (GLODAPv2). *Earth Syst. Sci. Data* 8, 297–323. <https://doi.org/10.5194/essd-8-297-2016>.
- Olsen, A., Lange, N., Key, R.M., Tanhua, T., Álvarez, M., Becker, S., Bittig, H.C., Carter, B. R., Cotrim da Cunha, L., Feely, R.A., Heuven, S. van, Hoppema, M., Ishii, M., Jeansson, E., Jones, S.D., Jutterström, S., Karlsen, M.K., Kozyr, A., Lauvset, S.K., Monaco, C.L., Murata, A., Pérez, F.F., Pfeil, B., Schirnack, C., Steinfeldt, R., Suzuki, T., Telszewski, M., Tilbrook, B., Velo, A., Wanninkhof, R., 2019. GLODAPv2.2019 – an update of GLODAPv2. *Earth Syst. Sci. Data* 11 (3), 1437–1461. <https://doi.org/10.5194/essd-11-1437-2019>.
- Ono, H., Kosugi, N., Toyama, K., Tsujino, H., Kojima, A., Enyo, K., Iida, Y., Nakano, T., Ishii, M., 2019. Acceleration of ocean acidification in the western north pacific. *Geophys. Res. Lett.* <https://doi.org/10.1029/2019GL085121>.
- Orr, J.C., Fabry, V.J., Aumont, O., Bopp, L., Doney, S.C., Feely, R.A., Gnanadesikan, A., Gruber, N., Ishida, A., Joos, F., Key, R.M., Lindsay, K., Maier-Reimer, E., Matear, R., Monfray, P., Mouchet, A., Najjar, R.G., Plattner, G.-K., Rodgers, K.B., Sabine, C.L., Sarmiento, J.L., Schlitzer, R., Slater, R.D., Totterdell, J.J., Weirig, M.-F., Yamanaka, Y., Yool, A., 2005. Anthropogenic ocean acidification over the twenty-first century and its impact on calcifying organisms. *Nature* 437 (7059), 681–686. <https://doi.org/10.1038/nature04095>.
- Orr, J.C., Epitalon, J.-M., Gattuso, J.-P., 2015. Comparison of ten packages that compute ocean carbonate chemistry. *Biogeosciences* 12 (5), 1483–1510. <https://doi.org/10.5194/bg-12-1483-2015>.
- Orr, J.C., Epitalon, J.-M., Dickson, A.G., Gattuso, J.P., 2018. Routine uncertainty propagation for the marine carbon dioxide system. *Mar. Chem.* 207, 84–107. <https://doi.org/10.1016/j.marchem.2018.11.006>.
- Pandolfi, J.M., Connolly, S.R., Marshall, D.J., Cohen, A.L., 2011. Projecting coral reef futures under global warming and ocean acidification. *Science* 333, 418–422. <https://doi.org/10.1126/science.1204794>.
- Pfeil, B., Olsen, A., Bakker, D.C.E., Hankin, S., Koyuk, H., Kozyr, A., Malczyk, J., Manke, A., Metz, N., Sabine, C.L., Akl, J., Alin, S.R., Bates, N., Bellerby, R.G.J., Borges, A., Boutin, J., Brown, P.J., Cai, W.-J., Chavez, F.P., Chen, A., Cosca, C., Fassbender, A.J., Feely, R.A., González-Dávila, M., Goyet, C., Hales, B., Hardman-Mountford, N., Heinze, C., Hood, M., Hoppema, M., Hunt, C.W., Hydes, D., Ishii, M., Johannessen, T., Jones, S.D., Key, R.M., Körtzinger, A., Landschützer, P., Lauvset, S. K., Lefevre, N., Lenton, A., Lourantou, A., Merlivat, L., Midorikawa, T., Mintrop, L., Miyazaki, C., Murata, A., Nakadate, A., Nakano, Y., Nakaoka, S., Nojiri, Y., Omar, A. M., Padin, X.A., Park, G.-H., Paterson, K., Perez, F.F., Pierrot, D., Poisson, A., Ríos, A. F., Santana-Casiano, J.M., Salisbury, J., Sarma, V.V.S.S., Schlitzer, R., Schneider, B., Schuster, U., Sieger, R., Skjelvan, I., Steinhoff, T., Suzuki, T., Takahashi, T., Tedesco, K., Telszewski, M., Thomas, H., Tilbrook, B., Tjiputra, J., Vandemark, D., Veness, T., Wanninkhof, R., Watson, A.J., Weiss, R., Wong, C.S., Yoshikawa-Inoue, H., 2013. A uniform, quality controlled Surface Ocean CO₂ Atlas (SOCAT). *Earth Syst. Sci. Data* 5, 125–143. <https://doi.org/10.5194/essd-5-125-2013>.
- Pierrot, D., Lewis, E., Wallace, D.W.R., 2006. MS Excel Program Developed for CO₂ System Calculations ORNL/CDIAC-105. Carbon Dioxide Inf. Anal. Cent., Oak Ridge Natl. Lab. U. S. Dept. of Energy, Oak Ridge, Tenn.
- Poisson, A., Metz, N., Brunet, C., Schauer, B., Bres, B., Ruiz-Pino, D., Louanchi, F., 1993. Variability of sources and sinks of CO₂ in the western Indian and southern oceans during the year 1991. *J. Geophys. Res.* 98 (C12), 22759–22778. <https://doi.org/10.1029/93JC02501>.
- Reynolds, R.W., Rayner, N.A., Smith, T.M., Stokes, D.C., Wang, W., 2002. An improved in situ and satellite SST analysis for climate. *J. Clim.* 15, 1609–1625. [https://doi.org/10.1175/1520-0442\(2002\)015<1609:AIASAS>2.0.CO;2](https://doi.org/10.1175/1520-0442(2002)015<1609:AIASAS>2.0.CO;2).
- Riebesell, U., Zondervan, I., Rost, B., Tortell, P.D., Zeebe, R.E., Morel, F.M.M., 2000. Reduced calcification of marine plankton in response to increased atmospheric CO₂. *Nature* 407 (6802), 364–367. <https://doi.org/10.1038/35030078>.
- Roxy, M.K., Ritika, K., Terray, P., Masson, S., 2014. The curious case of Indian ocean warming. *J. Clim. Am. Meteor. Soc.* 27 (22), 8501–8509. <https://doi.org/10.1175/JCLI-D-14-00471.1>.
- Sabine, C.L., Key, R.M., Johnson, K.M., Millero, F.J., Poisson, A., Sarmiento, J.L., Wallace, D.W.R., Winn, C.D., 1999. Anthropogenic CO₂ inventory of the Indian ocean. *Global Biogeochem. Cycles* 13 (1), 179–198. <https://doi.org/10.1029/1998GB900022>.
- Schlitzer, R., 2013. Ocean Data View. <http://odv.awi.de>.
- Schönberg, C.H.L., Fang, J.K.H., Carreiro-Silva, M., Tribollet, A., Wisshak, M., 2017. Bioerosion: the other ocean acidification problem. *ICES (Int. Council. Explor. Sea) J. Mar. Sci. fsw254* <https://doi.org/10.1093/icesjms/fsm254>.
- Swart, N.C., Lutjeharms, J.R.E., Ridderinkhof, H., de Ruijter, W.P.M., 2010. Observed characteristics of Mozambique Channel eddies. *J. Geophys. Res.* 115, C09006. <https://doi.org/10.1029/2009JC005875>.
- Takahashi, T., Olafsson, J., Goddard, J.G., Chipman, D.W., Sutherland, S.C., 1993. Seasonal variation of CO₂ and nutrients in the high-latitude surface oceans: a comparative study. *Global Biogeochem. Cycles* 7 (4), 843–878. <https://doi.org/10.1029/93GB02263>.
- Takahashi, T., Sutherland, S.C., Sweeney, C., Poisson, A., Metz, N., Tilbrook, B., Bates, N., Wanninkhof, R., Feely, R.A., Sabine, C., Olafsson, J., Nojiri, Y., 2002. Global sea-air CO₂ flux based on climatological surface ocean pCO₂, and seasonal

- biological and temperature effect. *Deep-Sea Res. II* 49 (9–10), 1601–1622. [https://doi.org/10.1016/S0967-0645\(02\)00003-6](https://doi.org/10.1016/S0967-0645(02)00003-6).
- Takahashi, T., Sutherland, S.C., Wanninkhof, R., Sweeney, C., Feely, R.A., Chipman, D. W., Hales, B., Friederich, G., Chavez, F., Sabine, C., Watson, A.J., Bakker, D.C., Schuster, U., Metzl, N., Yoshikawa-Inoue, H., Ishii, M., Midorikawa, T., Nojiri, Y., Körtzinger, A., Steinhoff, T., Hoppema, M., Olafsson, J., Arnarson, T.S., Tilbrook, B., Johannessen, T., Olsen, A., Bellerby, R., Wong, C., Delille, B., Bates, N., de Baar, H.J., 2009. Climatological mean and decadal change in surface ocean pCO₂, and net sea air CO₂ flux over the global oceans. *Deep-Sea Res. II* 56 (8–10), 554–577. <https://doi.org/10.1016/j.dsr2.2008.12.009>.
- Takahashi, T., Sutherland, S.C., Chipman, D.W., Goddard, J.G., Ho, C., Newberger, T., Sweeney, C., Munro, D.R., 2014. Climatological distributions of pH, pCO₂, total CO₂, alkalinity, and CaCO₃ saturation in the global surface ocean, and temporal changes at selected locations. *Mar. Chem.* 164, 95–125. <https://doi.org/10.1016/j.marchem.2014.06.004>.
- Tan, K., Zheng, H., 2020. Ocean acidification and adaptive bivalve farming. *Sci. Total Environ.* 701, 134794. <https://doi.org/10.1016/j.scitotenv.2019.134794>.
- Ternon, J.F., Roberts, M.J., Morris, T., Hancke, L., Backeberg, B., 2014. In situ measured current structures of the eddy field in the Mozambique Channel. *Deep Sea Res. Part II Top. Stud. Oceanogr.* 100, 10–26. <https://doi.org/10.1016/j.dsr2.2013.10.013>.
- Tierney, J.E., Abram, N.J., Anchukaitis, K.J., Evans, M.N., Giry, C., Kilbourne, K.H., Saenger, C.P., Wu, H.C., Zinke, J., 2015. Tropical sea surface temperatures for the past four centuries reconstructed from coral archives. *Paleoceanography* 30, 226–252. <https://doi.org/10.1002/2014PA002717>.
- Tilbrook, B., Jewett, E.B., DeGrandpre, M.D., Hernandez-Ayon, J.M., Feely, R.A., Gledhill, D.K., Hansson, L., Isensee, K., Kurz, M.L., Newton, J.A., Siedlecki, S.A., Chai, F., Dupont, S., Graco, M., Calvo, E., Greeley, D., Kapsenberg, L., Lebec, M., Pelejero, C., Schoo, K.L., Telszewski, M., 2019. An enhanced ocean acidification observing network: from people to technology to data synthesis and information exchange. *Front. Mar. Sci.* 6 <https://doi.org/10.3389/fmars.2019.00337>.
- Touratier, F., Azouzi, L., Goyet, C., 2007. CFC-11, $\Delta^{14}\text{C}$ and ^3H tracers as a means to assess anthropogenic CO₂ concentrations in the ocean. *Tellus B* 59 (2), 318–325. <https://doi.org/10.1111/j.1600-0889.2006.00247.x>.
- Tréguer, P., Le Corre, P., 1975. Manuel d'analyse des sels nutritifs dans l'eau de mer (utilisation de l'autoanalyseur II Technicon), second ed. L.O.C.U.B.O., Brest, 1975, p. 110.
- Tribollet, A., 2019. Rapport de campagne, Rotation du Marion Dufresne dans les Iles Eparses du 4 au 30 avril 2019, CONSORTIUM DE RECHERCHE TAAF « ILES EPARSEES 2017-2020 ». Rapport Interne LOCEAN, p. 15.
- Tribollet, A., 2020. Rapport d'activité intermédiaire 2019 : projet CLIM-EPARSEES. CONSORTIUM DE RECHERCHE TAAF "Iles Eparses 2017-2020, p. 8.
- Tribollet, A., Chauvin, A., Cuet, P., 2019. Carbonate dissolution by reef microbial borers: a biogeological process producing alkalinity under different pCO₂ conditions. *Facies* 65, 2. <https://doi.org/10.1007/s10347-018-0548-x>.
- Trnovsky, D., Stoltenberg, L., Cyronak, T., Eyre, B.D., 2016. Antagonistic effects of ocean acidification and rising sea surface temperature on the dissolution of coral reef carbonate sediments. *Frontiers in Mar. Sci.* <https://doi.org/10.3389/fmars.2016.00211>.
- Uppström, L.R., 1974. The boron/chlorinity ratio of deep-sea water from the Pacific Ocean. *Deep Sea Res. Oceanogr. Abstr.* 21, 161–162. [https://doi.org/10.1016/0011-7471\(74\)90074-6](https://doi.org/10.1016/0011-7471(74)90074-6).
- Van Heuven, S., Pierrot, D., Rae, J.W.B., Lewis, E., Wallace, D.W.R., 2011. MATLAB Program Developed for CO₂ System Calculations. ORNL/CDIAC-105b. Oak Ridge, TN: Carbon Dioxide Information Analysis Center. Oak Ridge National Laboratory, U. S. Department of Energy. https://doi.org/10.3334/CDIAC/otg.CO2SYS_MATLAB_v1.1.
- Waldbusser, G.G., Hales, B., Langdon, C.J., Haley, B.A., Schrader, P., Brunner, E.L., Gray, M.W., Miller, C.A., Gimenez, I., 2015. Saturation-state sensitivity of marine bivalve larvae to ocean acidification. *Nat. Clim. Change* 5 (3), 273–280. <https://doi.org/10.1038/NCLIMATE2479>.
- Weiss, R.F., Price, B.A., 1980. Nitrous oxide solubility in water and seawater. *Mar. Chem.* 8 (4), 347–359. [https://doi.org/10.1016/0304-4203\(80\)90024-9](https://doi.org/10.1016/0304-4203(80)90024-9).
- Westberry, T.K., Siegel, D.A., 2006. Spatial and temporal distribution of Trichodesmium blooms in the world's oceans. *Global Biogeochem. Cycles* 20, GB4016. <https://doi.org/10.1029/2005GB002673>.
- Wu, H., Dissard, D., Douville, E., Blamart, D., Bordier, L., Tribollet, A., Le Cornec, F., Pons-Branchu, E., Dapoigny, A., Lazareth, C.E., 2018. Surface ocean pH variations since 1689 CE and recent ocean acidification in the tropical south Pacific. *Nat. Commun.* 9, 2543. <https://doi.org/10.1038/s41467-018-04922-1>.
- Zinke, J., Loveday, B., Reason, C., Dullo, W.-C., Kroon, D., 2014. Madagascar corals track sea surface temperature variability in the Agulhas Current core region over the past 334 years. *Sci. Rep.* 4, 4393. <https://doi.org/10.1038/srep04393>.